CellPress

Developmental Cell
Resource

Combining Genetic Perturbations and Proteomics to Examine Kinase-Phosphatase Networks in *Drosophila* Embryos

Richelle Sopko,[1,*] Marianna Foos,[1,3] Arunachalam Vinayagam,[1] Bo Zhai,[2,4] Richard Binari,[1,3] Yanhui Hu,[1] Sakara Randklev,[1,3] Lizabeth A. Perkins,[1] Steven P. Gygi,[2] and Norbert Perrimon[1,3,*]
[1]Department of Genetics, Harvard Medical School, Boston, MA 02115, USA
[2]Department of Cell Biology, Harvard Medical School, Boston, MA 02115, USA
[3]Howard Hughes Medical Institute, Boston, MA 02115, USA
[4]Present address: St. Jude Children's Research Hospital, Memphis, TN 38105, USA
*Correspondence: rsopko@genetics.med.harvard.edu (R.S.), perrimon@receptor.med.harvard.edu (N.P.)
http://dx.doi.org/10.1016/j.devcel.2014.07.027

SUMMARY

Connecting phosphorylation events to kinases and phosphatases is key to understanding the molecular organization and signaling dynamics of networks. We have generated a validated set of transgenic RNA-interference reagents for knockdown and characterization of all protein kinases and phosphatases present during early *Drosophila melanogaster* development. These genetic tools enable collection of sufficient quantities of embryos depleted of single gene products for proteomics. As a demonstration of an application of the collection, we have used multiplexed isobaric labeling for quantitative proteomics to derive global phosphorylation signatures associated with kinase-depleted embryos to systematically link phosphosites with relevant kinases. We demonstrate how this strategy uncovers kinase consensus motifs and prioritizes phosphoproteins for kinase target validation. We validate this approach by providing auxiliary evidence for Wee kinase-directed regulation of the chromatin regulator Stonewall. Further, we show how correlative phosphorylation at the site level can indicate function, as exemplified by Sterile20-like kinase-dependent regulation of Stat92E.

INTRODUCTION

Despite the ease with which we can identify protein phosphorylation, in the vast majority of cases, the protein kinase(s) or phosphatase(s) responsible for controlling any particular phosphorylation event is unknown. We sought to develop a proteomic strategy to easily and systematically screen for candidate protein kinase and phosphatase substrates in *Drosophila melanogaster* embryos, with the goal of identifying specific residues that these enzymes target in the context of development. *D. melanogaster* is an ideal model for the dissection of signaling mechanisms, as the majority of transcription in the embryo occurs after the mid-blastula transition (MBT), and thus, transcriptional feedback has relatively no impact on the phosphoproteome in early embryos. Additionally, since the embryo is a syncytium prior to cellularization at the MBT, distortions in phosphosite measurements due to contributions from multiple cell types can be avoided. However, acquiring sufficient material from mutant embryos for proteomic studies is a challenge. The classical technique to generate maternally deficient embryos—relying on the production of germline clones using the flippase (FLP) recombinase-mediated dominant female sterile technique (Chou and Perrimon, 1996)—is labor intensive, as it involves the construction of complex genotypes. Moreover, background mutations on the FLP-recognition-target-bearing chromosome can confound phenotype interpretation, and the approach does not typically yield enough material for proteomic studies.

Here, we describe how we have used genetic manipulation by transgenic RNA interference (RNAi) to derive sufficient quantities of embryos for phosphoproteomic analyses. RNAi is a well-founded method to analyze gene function in *D. melanogaster* (Perrimon et al., 2010), but the efficacy of RNAi during early embryogenesis has only recently been improved to enable robust gene knockdown during this developmental stage (Ni et al., 2011). By using the Gal4/UAS system (Brand and Perrimon, 1993) to temporally and spatially restrict expression of RNAi reagents, we confined protein kinase and phosphatase knockdown specifically to the germline. Using this strategy, we were able to query maternal gene function without affecting the viability of the animal, since an intact germline is dispensable for organismal development. We generated and validated a transgenic RNAi library that targets all protein kinases and phosphatases expressed in the *D. melanogaster* germline. Through rigorous characterization of our collection, we uncovered maternal-effect genes and verified previously implicated kinases and phosphatases in early *D. melanogaster* development. Furthermore, we systematically monitored global phosphoproteome alterations in kinase-deficient embryos for the purpose of illustrating how the method can generate lists of candidate kinase substrates. The approach illuminated kinase-dependent signaling and permitted the unbiased prediction of kinase consensus motifs that match kinase specificities previously characterized in vitro. As anticipated, the strategy identified downregulated phosphoproteins that include bona fide kinase substrates of the depleted kinase and an extensive list of candidate kinase-targeted substrates and phosphosites. We further

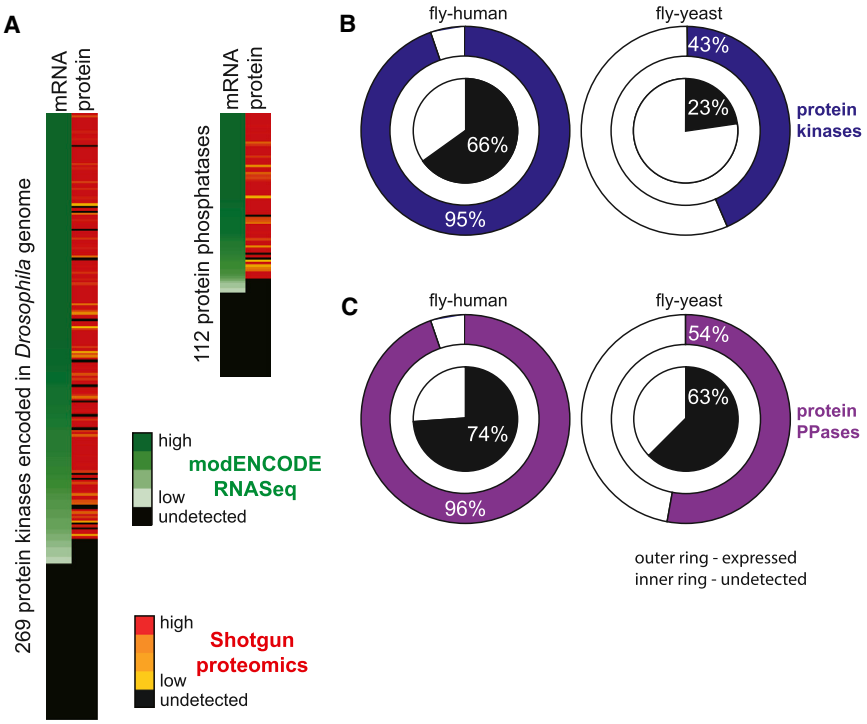

Figure 1. Expression and Conservation of Protein Kinases and Protein Phosphatases during Early *D. melanogaster* Embryogenesis

(A) Of 269 *D. melanogaster* protein kinase-encoding genes, 201 were identified by RNA-seq between 0 and 4 hr of embryogenesis, while 76 of 112 protein phosphatase-encoding transcripts were identified for the same developmental window. Represented is an average RPKM value from two time points comprising stages 1–8. Undetected transcripts are those with an RPKM value less than 3. Average RPKM values ranged from high (257: *polo*) to low (3: *btl*, *PVR*, and *CG43143*) for kinases and from high (327: *mts*) to low (3: *CG565* and *CG16771*) for phosphatases. Corresponding proteins, identified from MS2-based peptide fragmentation, were quantified based on label-free peptide MS1 feature intensities from shotgun mass spectrometry for the same developmental time. A total of 172 kinases and 67 phosphatases were quantified. Median signal-to-noise ratios observed across all matching peptides ranged from high (156: Cks30A) to low (5: CG7156) for kinases and from high (107: Pp2B-14D) to low (6: CG8147 and Ptp4E) for phosphatases.

(B) Conservation of expressed (outer ring) and undetected (inner pie) *D. melanogaster* protein kinases during early embryogenesis (0–4 hr) to human and yeast.

(C) Conservation of expressed (outer ring) and undetected (inner pie) *D. melanogaster* protein phosphatases during early embryogenesis (0-4 hr) to human and yeast. Conservation was considered when three or more ortholog predictions tools (DIOPT score > 3) predicted a high confidence ortholog.

See also Figure S1.

establish that two phosphosites consistently responding in the same direction (positive correlation) or the opposite direction (negative correlation) in different genetic contexts can illuminate phosphosite functionality. Given the extensive similarity between human and *D. melanogaster* kinases, and the conservation of functional phosphorylation (Gnad et al., 2010; Landry et al., 2009), we anticipate that insight gained from our data and analyses will inform future mammalian studies.

RESULTS

Compilation of the Maternally Inherited Protein Kinome and Phosphatasome

The *D. melanogaster* genome encodes 32 tyrosine kinases, 237 serine/threonine kinases, and 112 protein phosphatases (Manning et al., 2002; Morrison et al., 2000). To systematically link protein phosphorylation sites with their cognate kinases and phosphatases in *D. melanogaster*, we first identified the complement of kinase and phosphatase messenger RNAs (mRNAs) that are deposited maternally and contribute to the early zygote by analyzing developmental time course RNA sequencing (RNA-seq) data (Graveley et al., 2011). Using an RPKM (reads per kilobase of exon model per million mapped reads) cutoff of 3, determined by comparison to real-time quantitative PCR (qPCR) analysis of staged embryos (Hu et al., 2013b), we determined that 201 protein-kinase-encoding transcripts and 76 protein phosphatase-encoding transcripts (Figure 1A; Table S1 available online) are present during the first 4 hr of embryogenesis (stages 1–8). This accounts for 75% and 68% of all protein kinases and phosphatases, respectively, encoded in the *D. melanogaster* genome (Figure 1A). We independently verified the presence of these transcripts by real-time qPCR (Figure 2A) but detected only 172 kinases and 67 phosphatases in 2-hr-old embryos (stages 1–4) at the protein level based on peptide MS1 feature intensities from shotgun mass spectrometry (Figure 1A). Most kinases and phosphatases we identified as transcripts were reliably detected as protein. We found that, for only 28 kinases and 9 phosphatases where mRNA was identified, the corresponding protein at the appropriate time interval was not detected (Table S1). Thus, mRNA detection was generally a good predictor of protein presence. However, when considering levels rather than identity, we found no correlation between mRNA and protein (Figure S1), similar to observations from large-scale studies in *Schizosaccharomyces pombe* (Marguerat et al., 2012). Using a stringent criterion of conservation (i.e., at least three independent prediction tools support an orthologous gene-pair relationship; Hu et al., 2013a), we found that nearly all protein kinases and phosphatases expressed during early *D. melanogaster* development are conserved to human (Figures 1B and 1C; Table S1). On the contrary, conservation to yeast is far more limited.

Generation and Validation of the Transgenic shRNA Collection Targeting Kinases and Phosphatases

We previously demonstrated the utility of short hairpin RNAs (shRNAs) embedded in an endogenous microRNA scaffold to knock down maternal gene function in *D. melanogaster* embryos. A side-by-side comparison of shRNA with long double-stranded

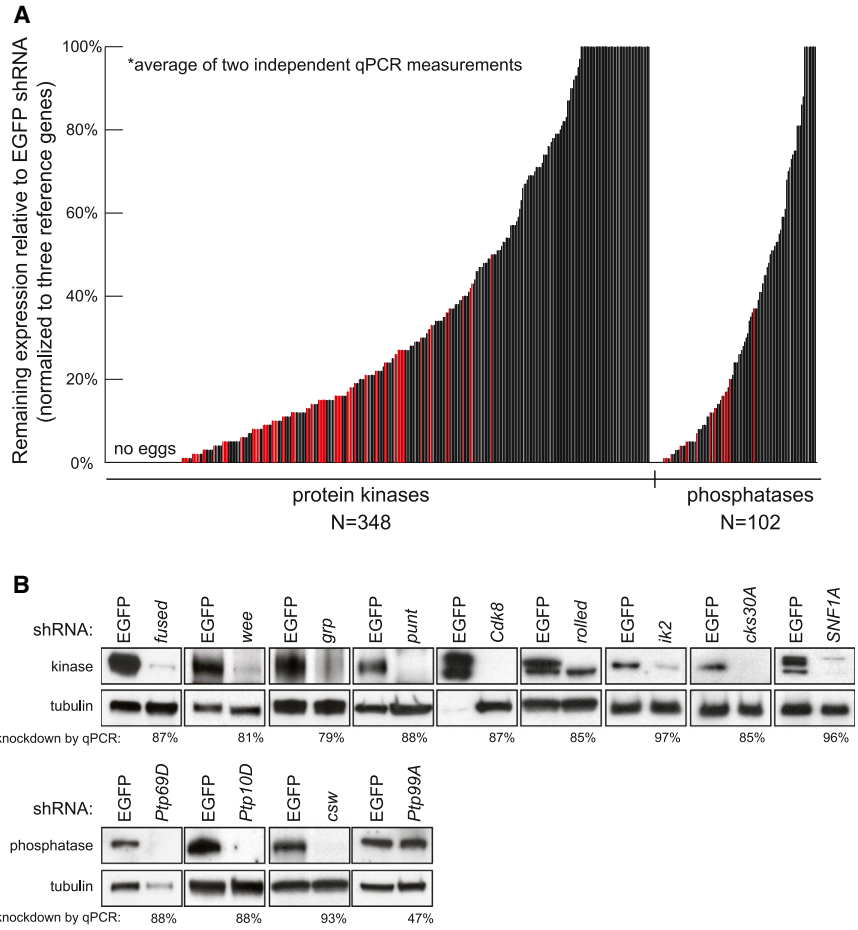

Figure 2. Knockdown Efficiency of Maternally Expressed shRNAs

(A) Plotted is the average remaining transcript level for individual protein kinases and phosphatases targeted by a specific shRNA, relative to a shRNA-targeting EGFP, as assessed by real-time qPCR. Three reference genes were used for normalization. Approximately 12% of the lines could not be analyzed, since germline knockdown of these genes induced female sterility (no eggs). Indicated in red are lines that generated phenotypes.

(B) Lysate from 0–4 hr embryos was subjected to immunoblotting, and levels of the corresponding kinase or phosphatase were assessed relative to tubulin. Indicated below the immunoblots is the extent of knockdown determined by RT-qPCR, achieved for the corresponding shRNA.

See also Figure S2.

RNA (dsRNA) transgenic lines indicates that screening of shRNA lines triples the frequency of RNAi-derived germline phenotypes (Yan et al., 2014), generally due to higher expression of shRNAs in the germline (Ni et al., 2011). Having characterized the requirements for efficient gene knockdown during oogenesis, we sought to generate a complete and validated set of shRNA-expressing transgenic lines capable of targeting protein kinases and phosphatases that are contributed maternally to the developing embryo. To induce shRNA expression specifically in the female germline using the Gal4-UAS system, we crossed females heterozygous for a UAS shRNA and either MTD-Gal4 (a line bearing three copies of Gal4 expressed sequentially throughout oogenesis; Petrella et al., 2007) or tub-Gal4 (a line bearing two insertions of Gal4 expressed from a maternal tubulin promoter during mid- and late oogenesis; Staller et al., 2013) to shRNA-bearing males in order to recover fertilized eggs. We analyzed more than 450 transgenic lines expressing shRNAs targeting protein kinases and phosphatases (Table S2). We were unable to recover eggs from ~12% of the lines crossed to MTD-Gal4, accounting for 46 kinases and 6 phosphatases and implying that these genes are required for early oogenesis.

For those lines from which we could recover eggs, we determined by real-time qPCR, following the Minimum Information for Publication of Quantitative Real-Time PCR Experiments guidelines (Bustin et al., 2009), that more than half of the ~450 transgenic lines we analyzed generated greater than 60% knockdown of corresponding kinase or phosphatase mRNA levels in 0-4 hr embryos, relative to a control shRNA targeting enhanced green fluorescent protein (EGFP) (Figures 2A and S2A). We observed excellent correlation between knockdown at the mRNA and protein level, which was assessed by comparing mRNA levels assessed by real-time qPCR to immunoblots of a subset of proteins for which antibodies were available (Figure 2B). We were interested in determining the number of transgenic lines that would need to be considered to observe at least one achieving >60% knockdown of the targeted transcript. We found that, when considering two unique shRNAs targeting the same gene product, this occurs at a frequency of 86% (N = 81 pairs) (Figure S2B). These data suggest that generating two independent shRNA lines is usually sufficient for obtaining at least one line that confers adequate knockdown. Interestingly, many cases of poor knockdown can be attributed to shRNA targeting design. Specifically, our data indicate that shRNAs targeting the transcript coding sequence (CDS) are more effective at knockdown than those targeting 3′ untranslated regions (UTRs) (Figure S2C), possibly reflecting inaccuracies in UTR annotation (Hu et al., 2013b).

Notably, we found no correlation between the degree of knockdown and the level of corresponding transcript in untreated early embryos (Figure S2D). Furthermore, our data exhibit no bias toward the concentration of recovered RNA or the date of sample collection (Figures S2E and S2F). Taken together, our collection consists of at least one transgenic line that provides a minimum of 60% knockdown for each maternally inherited protein kinase and phosphatase.

Assessment of Transgenic shRNA Collection Phenotypes

Our shRNA-directed knockdown strategy recapitulated many documented maternal-effect phenotypes (Figure 3A). As

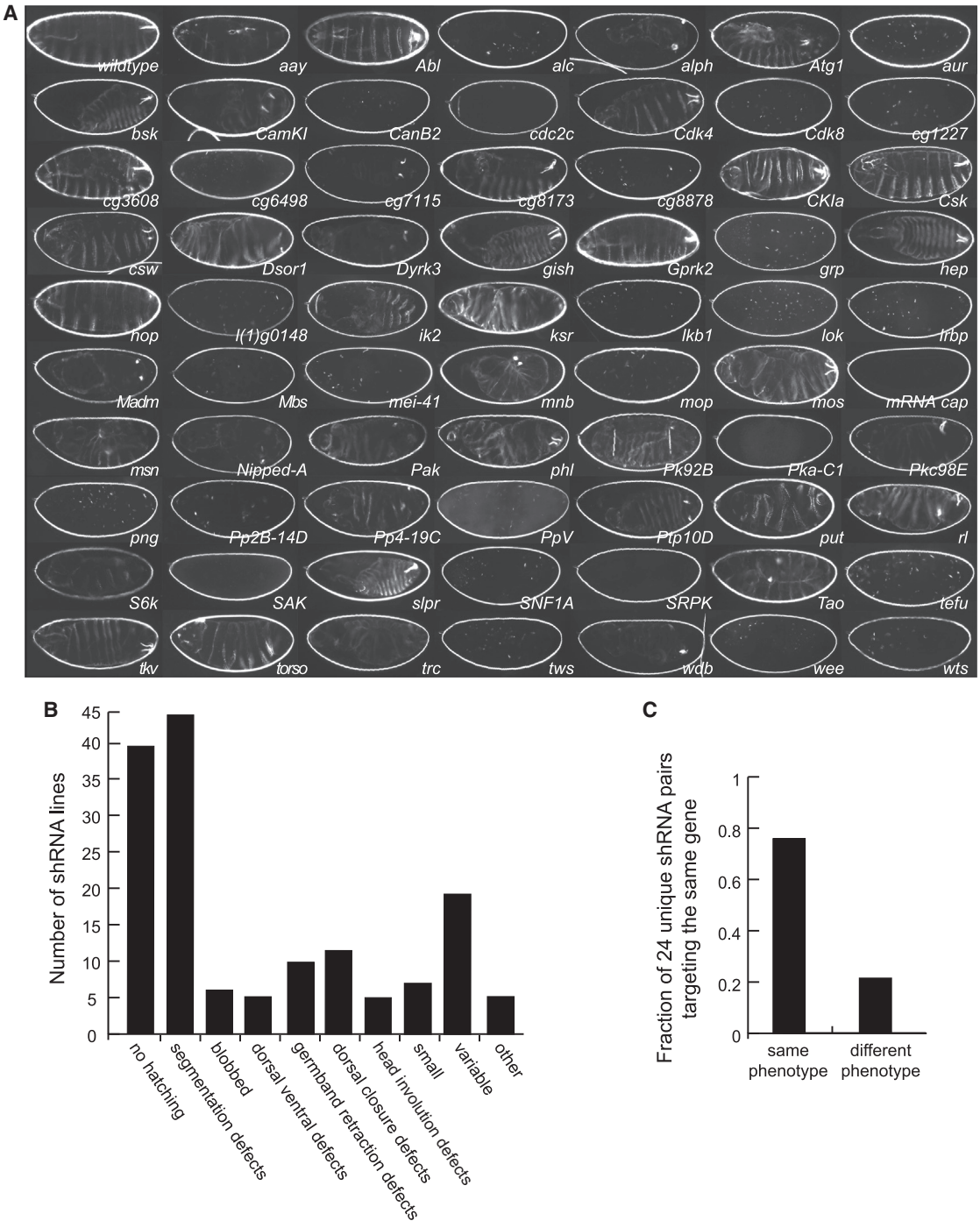

Figure 3. Embryonic Phenotypes Generated from shRNA-Mediated Knockdown of Maternally Contributed Protein Kinase and Phosphatases

(A) Cuticle phenotypes of embryos derived from maternal-Gal4>UAS-shRNA females crossed to UAS-shRNA males. Description of associated phenotypes can be found in Table S2.

(B) Frequency of observed embryonic phenotypes derived from maternal-Gal4/UAS-shRNA females crossed to UAS-shRNA males, from of a total of 450 examined lines.

(C) Twenty-four pairs of shRNAs targeting the same gene and generating >60% knockdown were compared for qualitatively similar embryonic phenotypes. Four of the six cases of a differential phenotype can be explained by degree of knockdown.

See also Table S2.

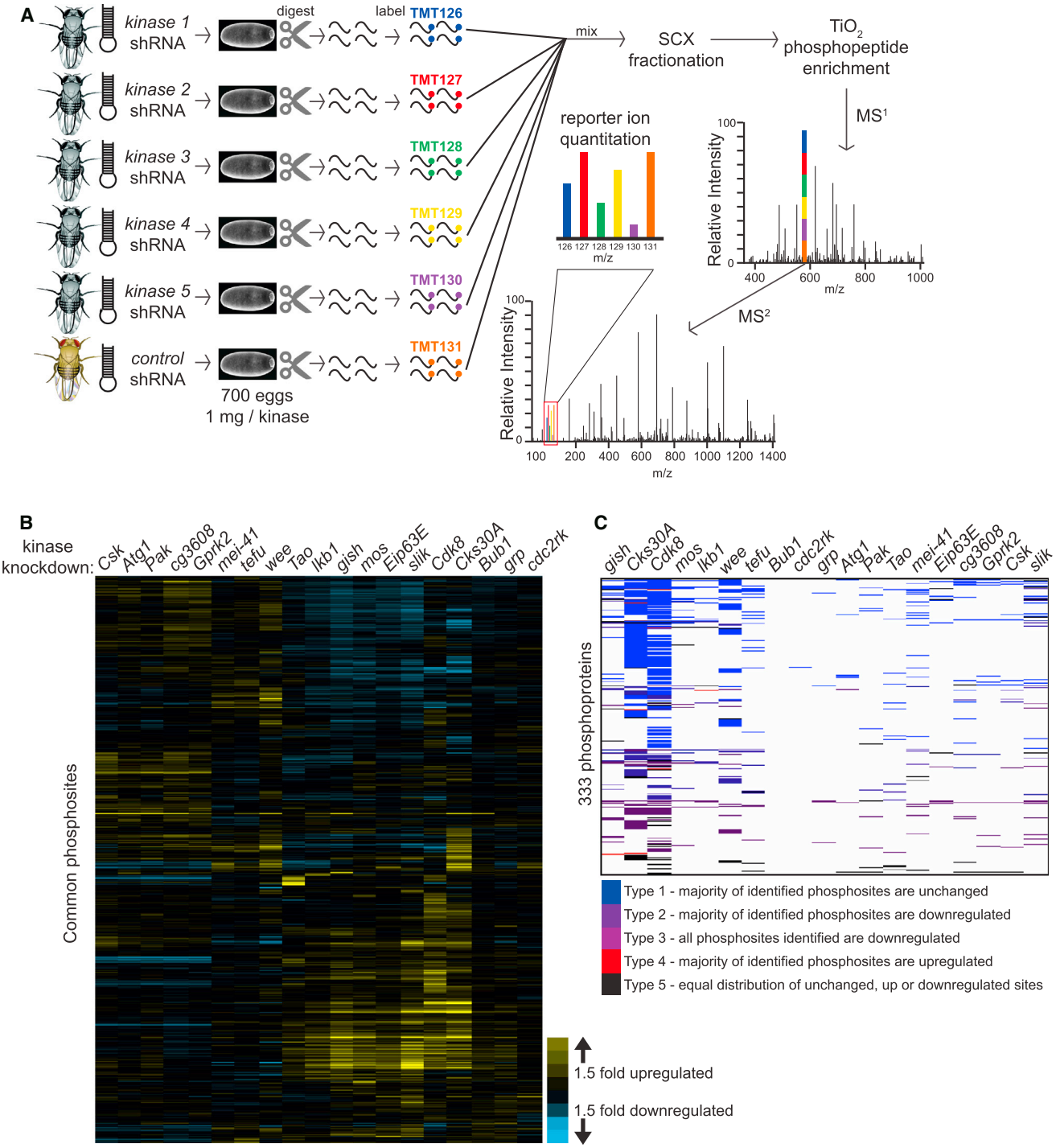

Figure 4. Phosphoprofiles of Kinase-Deficient *D. melanogaster* Embryos Generated by Quantitative Mass Spectrometry and Isobaric Labeling with Tandem Mass Tags

(A) Strategy followed to identify differential phosphorylation between kinase shRNA and control shRNA embryos (see Supplemental Experimental Procedures for details).

(B) Relative phosphosite levels between kinase shRNA and control shRNA embryos. Plotted is the fold change relative to a control shRNA (*white*) for phosphosites found among all experiments. These 1,139 unique phosphopeptides meet stringent criteria in terms of isolation specificity and phosphosite assignment (see Experimental Procedures). The hierarchical 2D matrix is clustered based on a correlation distance metric using average linkage. Knockdown efficiencies are as follows: *Cdk8*, 87%; *Cks30A*, 85%; *slik*, 92%; *wee*, 81%; *Tao*, 91%; *mei-41*, 84%; *tefu*, 68%; *lkb1*, 86%; *Atg1*, 92%; *Bub1*, 99%; *grp*, 79%; *cg3608*, 89%; *Gprk2*, 82%; *cdc2rk*, 85%; *gish*, 58%; *mos*, 90%; *Csk*, 90%; *Pak*, 95%; *Eip63E*, 71%.

(legend continued on next page)

expected, we observed anterior-posterior terminal defects following the disruption of terminal signaling, such as that resulting from knockdown of the receptor tyrosine kinase *torso*, the SHP2 phosphatase ortholog *corkscrew*, or the downstream kinase suppressor of ras, *ksr* (Figure 3A). Altogether, we observed maternal-effect phenotypes for ~18% of lines that achieved 60% or greater knockdown (Figure 3B; Table S2), representing approximately 33% and 18%, respectively, of protein kinases and phosphatases expressed during early embryogenesis. Of those protein kinases and phosphatases for which a maternal-effect phenotype has been reported, we observed the same qualitative phenotype as that described in the literature approximately 74% of the time (26/35 genes considering germline clone-derived embryos; 2/3 considering embryos derived from homozygous mutant mothers; Table S3A). Anomalies can likely be attributed to: (1) weak hypomorphic alleles generating a less severe phenotype than extensive knockdown; (2) insufficient knockdown by an shRNA to produce phenotypes generated by strong or null mutant alleles; or, (3) in the case of embryos derived from mutant mothers, an effect resulting from mutant somatic follicular cells. Despite the fact that protein kinases and phosphatases are among the best characterized classes of genes, we uncovered unappreciated phenotypes for approximately 40 of these enzymes, implying roles in oogenesis and early embryogenesis. Further, knockdown of an additional 12 predicted kinases and phosphatases resulted in oogenesis and maternal-effect phenotypes, warranting more extensive characterization. A searchable interface to query genes for individual transgenic lines, a description of their knockdown and embryonic phenotypes, and photos of cuticle preparations for those with maternal-effect phenotypes can be found at http://www.flyrnai.org/RSVP.html.

We addressed the possibility and frequency of shRNAs generating phenotypes as a result of off-target effects (OTEs) in two ways. First, we compared pairs of unique shRNAs targeting the same gene for similar phenotypes. Comparing 24 efficient targeting pairs, we found that 80% produced the same qualitative phenotype (Figure 3C; Table S3B). Four of the six cases of a differential phenotype can be explained by the extent of knockdown. Second, we established transgenic lines expressing "C911" versions of a targeting shRNA: a near-identical shRNA but with complementary nucleotides situated at positions 9–11. The mismatched shRNA precludes on-target binding while maintaining off-target binding since antisense and sense seed sequences remain intact (Buehler et al., 2012). Consistent with phenotypes resulting from on-targeting specificity provided by perfect complementary of the shRNA, we eliminated phenotypes resulting from expression of 16 unique shRNAs by mutating the central three nucleotides of the shRNA. We verified by real-time qPCR that mutation of these three residues eliminated knockdown of corresponding kinase transcripts that the shRNA originally targeted (data not shown). Thus, we conclude that the prevalence of OTEs affecting early embryogenesis is minimal with the shRNA targeting strategy.

A Resource Providing Accessibility for Proteomic Analyses and Kinase Characterization

Our current reagents for germline-specific RNAi make it relatively easy to obtain large numbers of eggs depleted of a single gene product. This allowed us to perform quantitative proteomic experiments to measure the global effect of each perturbation on the phosphoproteome (Figure 4A). We anticipated that a relative quantitative and global assessment of altered phosphorylation in protein kinase-deficient embryonic extracts could provide a list of putative protein kinase-substrate (KS) and phosphosite matches. We also reasoned that phosphorylation signatures could also be used to predict roles for protein kinases and phosphatases in specific biological processes and reveal functional redundancy.

We initially assessed the reproducibility of phosphoproteomic profiles generated from analysis of separate populations of control shRNA embryos. We utilized mass spectrometry and an isobaric labeling strategy (see the Protocol) that enables multiplexing and relative quantification between samples (see Supplemental Experimental Procedures). Since ~700 embryos constitute the amount of material (~1 mg protein) we chemically label, the phosphoproteomic profile is a representative average of phosphorylation in this population. Amine-reactive TMT Isobaric Mass Tags, identical in mass but differing in their isotopic distribution of atoms, permit the simultaneous spectral identification of unique reporter ions generated from MS2-based fragmentation of each tag from labeled peptides. We compared TMT reporter ion intensities and phosphopeptide identities from three TMT-labeled control shRNA embryo populations in two independent experiments (Table S4). When considering those phosphopeptides in the same multiplex experiment (10,166 phosphopeptides for one experiment and 8,032 for the other; see Supplemental Experimental Procedures for normalization and specific criteria), we generally identify the same phosphopeptide in all three biological replicates (~99% of the time). In the two independent experiments, we observed phosphopeptide levels deviating an average of 7% (Figure S3A) and 29% (Figure S3B) between three biological replicates. This indicates that variability in factors such as peptide labeling and embryo collection has little influence on our ability to consistently detect the majority of phosphopeptides.

Given the reproducibility between control shRNA replicates, we extended our phosphoproteomic examination to embryos derived from females expressing efficient shRNAs (as determined by real-time qPCR) targeting 19 different protein kinases (Figure 4B). We were able to quantify nearly 8,500 unique phosphosites among 19 deficient kinase samples (Tables S5A–S5D). The number of unique phosphosites we quantified between experiments, ranging from 6,331 to 2,448, was based on the number of unique phosphopeptides identified per experiment, ranging between 22,942 and 12,201. Notably, 1,140 phosphosites were quantified in all 19 kinase knockdown conditions, 1,343 in ten kinase knockdown conditions, and 4,358 in five kinase knockdown conditions. The majority of phosphopeptides

(C) Phosphoproteins with two or more downregulated phosphosites (>1.5-fold) were classified into four types based on the directionality of change of the majority of identified phosphosites for the same protein: type 1, most identified phosphosites do not change; type 2, most identified phosphosites are downregulated; type 3, all identified phosphosites are downregulated; and type 4, most identified phosphosites are upregulated.
See also Figures S3 and S4.

in each kinase-deficient sample were unchanging in abundance relative to the same control shRNA included in each multiplex experiment. In terms of candidate kinase-targeted phosphosites, either direct or indirect, we consider those downregulated sites with changes of 1.5-fold or greater in kinase-deficient embryos relative to control embryos, since observed phosphopeptides for seven shRNA-targeted kinases—Wee, Tao, Atg1, Gilgamesh (Gish), Lkb1, Grapes (Grp), and Sterile20-like kinase (Slik)—minimally met this criterion (2.27-fold, 1.95-fold, 1.69-fold, 2.24-fold, 2.68-fold, 1.98-fold, and 2.1-fold, respectively) in corresponding kinase-deficient embryos (Figure S4A). We did not detect phosphopeptides for the other 12 shRNA-targeted kinases. Moreover, changes in the phosphorylation of known substrates of shRNA-targeted kinases approach this value; for instance, Histone H3, Med13, and Stat92E (downregulated 2.2-fold, 1.8-fold, and 2.4-fold, respectively) in *Cdk8*-deficient embryos and Cdk1, Klp61F, and Hsp83 (downregulated 1.4-fold, 2.1-fold, and 1.7-fold, respectively) in *wee*-deficient embryos. Indeed, for a third of the *D. melanogaster* orthologs of literature-curated Cdk8 substrates in yeast (Sharifpoor et al., 2011) we identified, one or more respective phosphopeptides were downregulated >1.5-fold in *Cdk8*-deficient embryos (Table S5E). Using this criterion, the number of downregulated phosphosites in kinase-deficient profiles ranged from 22 (*Bub1*-deficient embryos) to 752 (*Cdk8*-deficient embryos) (Table S5). Of note, while our *Bub1*-targeting shRNA generated efficient knockdown (99% knockdown), *Bub1*-deficient embryos exhibited no morphological or hatch rate defects (Table S2), consistent with minimal effects on the phosphoproteome. Conversely, knockdown of *Cdk8*, a cyclin-dependent kinase influencing transcription and cell cycle progression (Szilagyi and Gustafsson, 2013), resulted in dramatic and penetrant morphological and hatch rate phenotypes, consistent with extensive modulation of the observed phosphoproteome. We speculate that among those phosphosites downregulated >1.5-fold in the 19 kinase-deficient contexts we surveyed are sites directly targeted by the corresponding depleted kinase(s), as well as indirect targets altered downstream of the manipulated kinase. For instance, in the case of *gish*-deficient embryos, we observed enrichment of downregulated phosphorylation of proteins involved in Hedgehog (Hh) and Wnt/Wingless (Wg) pathways (Table S5B), consistent with a role for Gish in mediating Hh and Wg signaling (Davidson et al., 2005; Hummel et al., 2002). These data indicate that, by monitoring changes in the phosphoproteome, one can effectively screen for candidate substrates and alterations in signaling downstream of the targeted kinase. However, further scrutiny of any altered phosphosite is required to prove a KS relationship, as we demonstrate later.

In order to distinguish genuine kinase targets from phosphosite alterations due to protein instability, we classified phosphoproteins with two or more downregulated phosphosites (>1.5-fold) into five categories based on the directionality of change of the majority of identified phosphosites for each individual protein: type 1, the majority of phosphosites do not change; type 2, the majority of phosphosites are downregulated; type 3, all phosphosites are downregulated; type 4, most phosphosites are upregulated; and type 5, indistinguishable due to an equal distribution of unchanged, upregulated, or downregulated phosphosites (Figure 4C). In considering at least two phosphosites, we increase the probability that the corresponding phosphoprotein is indeed subjected to degradation and not merely reduced in phosphorylation at a single site. Type 1 and type 4 phosphoproteins are those for which we can reasonably discount the possibility of protein degradation as a mechanism of downregulated phosphorylation and, thus, are considered high-priority candidates for phosphorylation by the respective kinase. The observed downregulation of type 3 phosphoproteins, on the other hand, can be explained by indirect mechanisms leading to protein degradation, such as altered protein-protein interactions or phosphorylation-mediated degradation. Although most phosphoproteins in our data set are of type 1 (Figure 4C), type 3 phosphoproteins account for ~20%, on average, of those proteins with two or more downregulated phosphosites in each kinase depletion condition. This percentage is in line with previous reports that protein expression changes account for less than 25% of differential phosphorylation (Bodenmiller et al., 2010; Wu et al., 2011). We scrutinized respective transcripts for type 2 and type 3 phosphoproteins in order to identify and filter our data set of potential OTEs due to partial complementarity of the targeting shRNA to unintended transcripts. By comparison to the frequency of partial complementarity of each targeting shRNA (seven-nucleotide match to seed) to the early embryonic transcriptome, we find a relatively weak probability for partial complementarity of our targeting shRNAs to 3′ UTRs or transcripts of type 2 phosphoproteins (see Supplemental Information). This probability declines when considering type 3 phosphoproteins, indicating that off-targets are not enriched in our data set and are therefore unlikely to explain alterations observed in our analyses. To further substantiate this assumption, we proceeded to knock down respective transcripts for type 3 phosphoproteins with the best matches to each corresponding kinase shRNA seed. Germline-specific knockdown of ten candidate off-targets predicted for six kinase-targeting shRNAs failed to generate phenotypes that could explain specific phenotypes attributed to the corresponding kinase shRNA (see Supplemental Information).

Extracting Patterns in Phosphorylation Data Sets to Find KS Relationships

We speculated that we might be able to extract KS relationships and insight into signaling pathway connectivity from our phosphorylation data set as a whole by examining patterns in phosphoalterations among kinase-deficient contexts. For instance, since most kinases are activated by phosphorylation, correlative phosphorylation events observed between kinases and other proteins could be indicative of KS relationships. On the other hand, anticorrelative phosphorylation could be additionally informative; inhibitory phosphorylation of a kinase would always be out of phase with phosphorylation of that kinase's respective targets. To explore such possibilities, we surveyed correlations in phosphorylation changes (>1.5-fold cutoff relative to a control shRNA) between identified phosphosite pairs among our kinase-deficient conditions (447,585 correlative pairs involving 2,058 phosphosites; Table S6A). When considering phosphosite pairs exhibiting positive or negative correlation in at least four kinase-deficient conditions (25,077 correlative pairs), we find enrichment for authentic KS pairs (Figure 5A), derived from 133,051 *D. melanogaster* KS pairs (Table S6B) predicted from

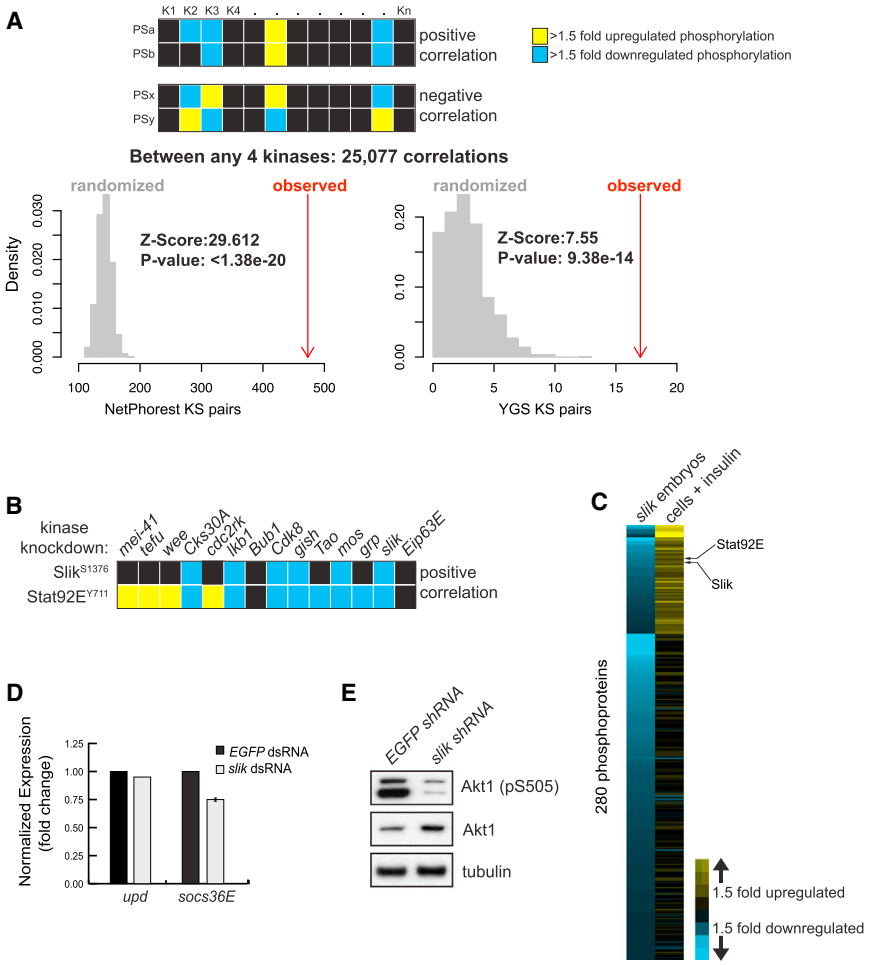

Figure 5. Correlative Phosphorylation Analysis Enriches for KS Pairs and Can Reveal Signaling Mechanisms

(A) Positive and negative correlations in phosphorylation changes (>1.5-fold relative to a control shRNA) between any two phosphosites (PS) were extracted from kinase-deficient phosphorylation profiles. Yeast gold standard (YGS) KS pairs (Sharifpoor et al., 2011) were mapped to *D. melanogaster* using DIOPT (Hu et al., 2011). *D. melanogaster* KS pairs were also predicted based on human kinase phosphorylation motifs from the NetPhorest atlas (Miller et al., 2008). The distribution of expected overlap between KS pairs and 1,000 simulated random correlation pairs of the same size is shown, and the overlap is shown in gray. The number of KS pairs observed among all correlation pairs is indicated (red arrow). Illustrated is the number of pairs when requiring phosphosite correlations among at least four kinase-deficient phosphorylation profiles. *Z* scores and p values are indicated.

(B) For those kinase-deficient embryonic lysates where phosphopeptides encompassing Slik^{S1376} and Stat^{Y711} were detected, we observed a positive correlation in the direction of alteration for these two phosphosites, relative to control.

(C) Comparison of common phosphoproteins in *slik*-deficient embryos (exhibiting >1.3-fold downregulation compared to control embryos) to *Drosophila* cells following 10–30 min insulin stimulation.

(D) The expression of Stat target genes *upd* and *socs36E* in *Drosophila* cells subjected to *slik* knockdown and stimulated with Upd ligand. Error bars indicate SEM.

(E) Activated Akt1 (phosphorylation at Ser505) levels in 0–4 hr *slik*-deficient embryos. Total Akt1 and tubulin serve as loading controls.

See also Figure S5.

179 conserved human kinase phosphorylation motifs by NetPhorest (Miller et al., 2008) and from mapping of 517 gold standard KS pairs in yeast (Sharifpoor et al., 2011) to *D. melanogaster*. Enrichment for authentic KS pairs still exists when considering phosphosite pairs correlating in only two or three kinase-deficient conditions (Figure S5A). Strikingly, we also find enrichment for correlative phosphorylation among components of the same protein complex ($p = 7.5 \times 10^{-157}$), further substantiating how this phenomenon can be exploited to identify functionally relevant phosphosites.

While correlative analysis can clearly illuminate direct KS relationships in large-scale phosphorylation data, it can also provide functional information if one has a priori knowledge of the consequence of phosphorylation of one of the participating phosphosites. We exemplify this with the case of Slik and Stat92E. Phosphorylation of the Stat92E transcription factor at Tyr711 promotes DNA binding (Yan et al., 1996). We found that phosphorylation at this particular site positively correlates with phosphorylation of Slik at Ser1376 (Figure 5B), suggestive of a relationship between Slik and Stat92E; the probability of observing two phosphosites correlating among six kinase-deficient profiles is rare ($p = 1.4 \times 10^{-5}$). We predicted that Slik activates Stat92E given that reduced Stat92E phosphorylation in *slik*-deficient embryos (Figure 5C) cannot be explained by instability of Stat92E protein (Figure S5B). Indeed, Stat92E target gene expression was downregulated in *slik* dsRNA-treated cells (Figure 5D). Insulin has been reported to enhance growth hormone-induced Stat activation in mature adipose cells (Zhang et al., 2013), and Stat may be a direct target of the insulin receptor (Sawka-Verhelle et al., 1997). We confirmed an increase in the activating phosphorylation of Stat92E in cells treated with insulin (Figure 5C). Remarkably, we observed that more than a quarter of phosphoproteins downregulated in *slik*-deficient embryos are upregulated in cells in response to insulin, including Slik (Figure 5C; Figures S5E and S5F). Moreover, 30% of phosphoproteins downregulated >1.3-fold in *slik*-deficient embryos (Table S7) were found to physically interact with components of the insulin-signaling network (Glatter et al., 2011). These observations suggest that Slik could be activating Stat92E via insulin signaling. Consistent with this, we observed a reduction in activated Akt1 in *slik*-deficient embryos, despite elevated total Akt1 protein (Figure 5E). A reduction in insulin signaling may, in fact, explain the longevity of *slik*^{1} mutant larvae (Hipfner and Cohen, 2003). Raf interaction has been suggested to bridge Slik to the MAPK proliferation branch of cell survival signaling (Hipfner and Cohen, 2003), which our data support, as we find that

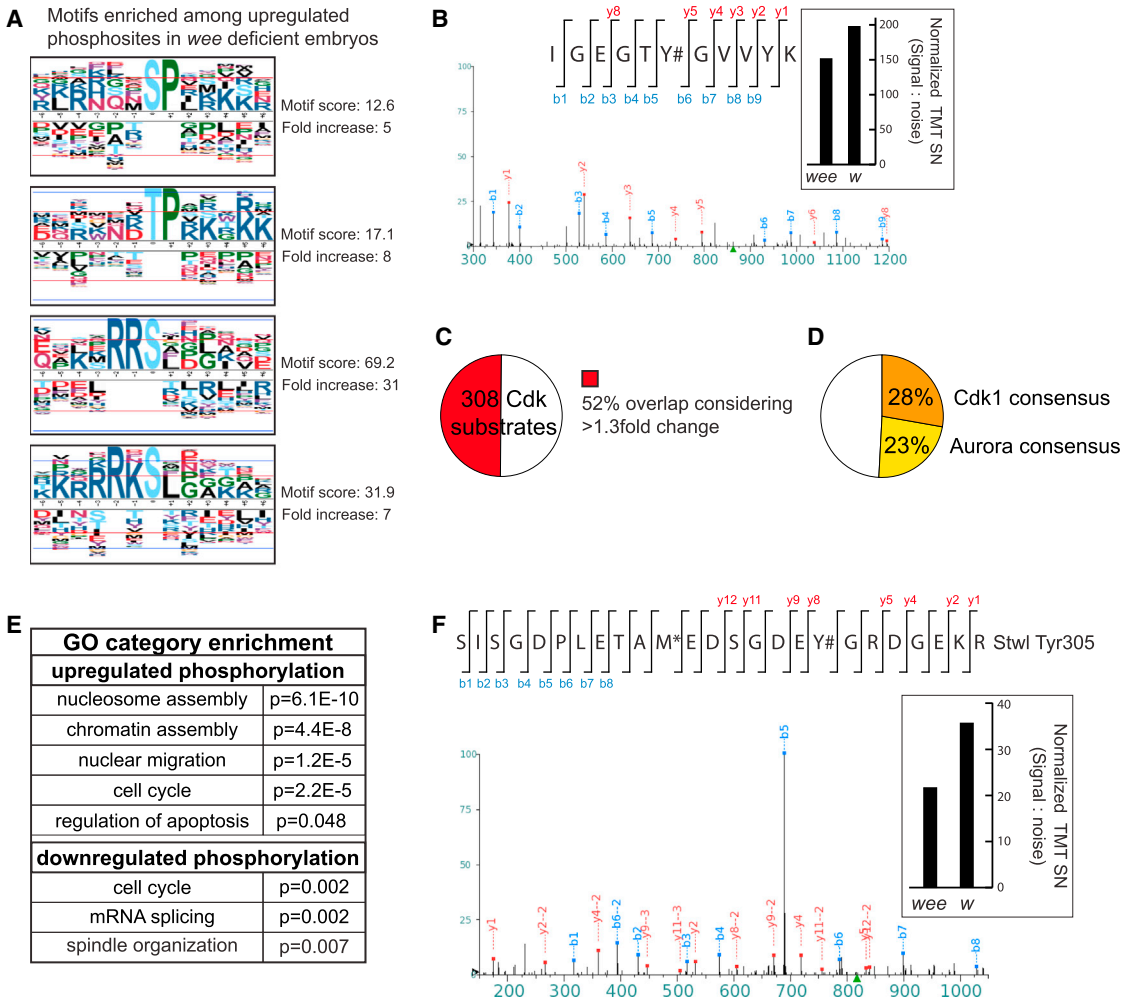

E

GO category enrichment	
upregulated phosphorylation	
nucleosome assembly	p=6.1E-10
chromatin assembly	p=4.4E-8
nuclear migration	p=1.2E-5
cell cycle	p=2.2E-5
regulation of apoptosis	p=0.048
downregulated phosphorylation	
cell cycle	p=0.002
mRNA splicing	p=0.002
spindle organization	p=0.007

Figure 6. Phosphoproteomic Characterization of *wee*-Deficient Embryos

(A) Indicated are motifs encompassing phosphosites that are enriched among phosphosites altered >1.5-fold in *wee*-deficient embryonic lysates relative to control. Motif-X was used to identify motifs (Chou and Schwartz, 2011). The PLogo tool was used to generate motif logos. Favored amino acids at corresponding positions are indicated above the black line, while disfavored amino acids are below. "0" indicates the site of phosphorylation.

(B) Levels of a Cdk1 Tyr15 encompassing phosphopeptide in *wee*-deficient embryos relative to control embryos (*w*, *white*) as determined by TMT reporter ion signal (right) from the corresponding peptide identified by MS2 fragmentation (left, MS2 spectra). The hashtag indicates the localized site of phosphorylation ($p < 0.05$). Indicated is a representative peptide.

(C) Of 308 phosphoproteins identified as Cdk1 substrates in yeast (Holt et al., 2009), we mapped 120 to fly with a DIOPT score ≥ 1. Half of the orthologous *D. melanogaster* counterparts exhibit altered phosphorylation (>1.3-fold) in *wee*-deficient embryos.

(D) Approximately half of those phosphosites upregulated >1.3-fold in *wee*-deficient kinases can be attributed to Cdk and the downstream kinase Aurora based on kinase consensus motif matching.

(E) Gene Ontology Consortium term enrichment among altered phosphoproteins (>1.5-fold) in *wee* shRNA embryos relative to control embryos, identified using the DAVID Functional Annotation Tool.

(F) Levels of a Stwl Tyr305 encompassing phosphopeptide in *wee*-deficient embryos relative to control embryos (*w*, *white*) as determined by TMT reporter ion signal (right) from the corresponding peptides identified by MS2 fragmentation (left, MS2 spectra). The hashtag indicates the site of phosphorylation ($p < 0.05$).

slik-deficient embryos exhibit defects in ERK activation (Figure S5D). Despite a nonessential role for *slik* in embryogenesis, our examination of correlative phosphorylation during this early stage illuminated Slik function, highlighting the power of our approach.

An Examination of Wee-Dependent Phosphorylation

We chose to examine more closely the phosphoproteomic profile of RNAi-derived *wee* kinase-deficient embryos, since their phenotype mirrored that reported for mutant *wee* embryos (Price et al., 2000). Wee, Cdk1, and Aurora operate in a regulatory kinase cascade to control nuclear divisions in the early embryo. Phosphorylation and activation of Aurora by Cdk1 is inhibited by Wee and delays entry into mitosis. Wee inhibits Cdk1 by phosphorylating a conserved tyrosine (Tyr15) located in the ATP binding pocket (Campbell et al., 1995; Stumpff et al., 2004). Therefore, we expected Cdk1 and Aurora to be hyperactive in the absence of Wee. Indeed, we find motif enrichment (Figure 6A) among

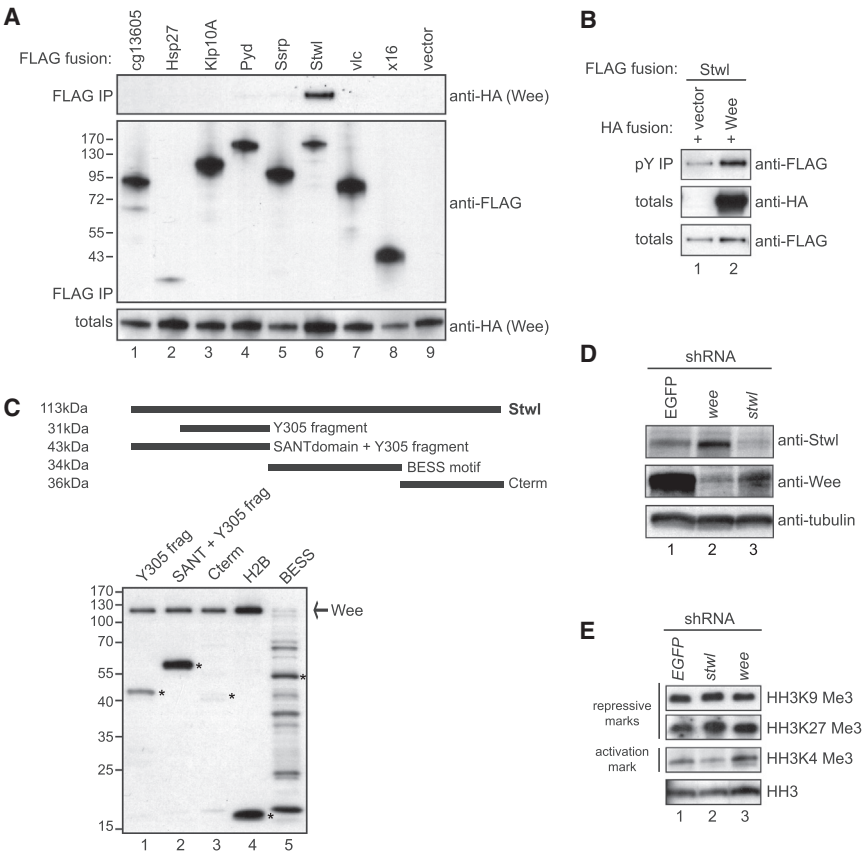

Figure 7. Identification of Stwl as a Target of Wee Kinase

(A) Lysates from *Drosophila* cells expressing HA-tagged Wee together with 3xFLAG-tagged candidate Wee substrates were subjected to immunoprecipitation with anti-FLAG antibody and analyzed by immunoblotting with the indicated antibodies.

(B) Lysates from *Drosophila* cells expressing HA-tagged Wee together with 3xFLAG-tagged Stwl were subjected to immunoprecipitation with anti-phosphotyrosine antibody and analyzed by immunoblotting with the indicated antibodies.

(C) Recombinant GST-Stwl fusion proteins were incubated with human WEE1 kinase and radiolabeled ATP and analyzed by SDS-PAGE and autoradiography. Histone H2B serves as a positive control (lane 4). The migration of input proteins is indicated with asterisks. Autophosphorylated WEE1 migrates at 120 kDa.

(D) Lysates from 0–2 hr embryos derived from females expressing shRNAs targeting *wee*, *stwl*, or an EGFP control shRNA were analyzed by immunoblotting with anti-Stwl and anti-Wee antibodies. Immunoblotting with anti-tubulin serves as a loading control.

(E) Lysates from 0–2 hr embryos derived from females expressing shRNAs targeting *wee*, *stwl*, or an EGFP control shRNA were analyzed by immunoblotting with antibodies recognizing different histone H3 posttranslational modifications.

upregulated phosphosites in *wee*-deficient embryos that resembles Cdk and Aurora kinase consensus motifs (Cdk1: pS/T-P-X-K/R; pS/T-P-X-X-K and Aurora: R-R/K-pS/T; R/K-X-pS/T; R-R/K-X-pS/T) (Alexander et al., 2011). Accordingly, we consistently observed less TMT reporter ion signal proportionate to levels of Cdk1 Tyr15 phosphopeptides in *wee*-deficient embryos, implying Cdk1 hyperactivity in this context (Figure 6B). We corroborated this observation by immunoblotting with a Cdk1-pTyr15 antibody (Figure S6A). Significantly, we identified altered phosphorylation on half of those fly proteins whose orthologous yeast counterparts were identified as Cdk substrates (Figure 6C) (Holt et al., 2009). Aurora is also hyperactive in *wee*-deficient embryos, reflected by the upregulation in phosphorylation of characterized targets: kinesin-like protein at 10A (Klp10A pSer210: 2.5-fold), inner centromere protein (Incenp pSer163: 1.5-fold and pSer164: 3-fold), and histone H3 (HH3 pSer10: 15-fold; pSer28: 7-fold) (Adams et al., 2001; Jang et al., 2009; Kang et al., 2001). We verified HH3 phosphoalterations in *wee*-deficient embryos by immunoblotting (Figure S6A). Surprisingly, half of the upregulated phosphosites we identified in *wee* kinase-deficient embryos reside within sequence recognized by Cdk1 or downstream Aurora kinase (Figure 6D). This observation highlights the utility of phosphoproteomic signatures to reveal genetic epistasis. We also find enrichment for specific Gene Ontology Consortium categories for those phosphoproteins regulated by Wee (Figure 6E). As anticipated, we observed enrichment for cell cycle classified factors, particularly those with mitosis-specific functions such as nuclear migration, spindle organization, and chromosome segregation. Intriguingly, proteins with roles in chromatin assembly are overrepresented in our list of upregulated phosphoproteins in *wee*-deficient embryos. This is interesting, given the reported hypocondensation of mitotic chromatin in *wee* null embryos (Stumpff et al., 2004). Motif enrichment among downregulated phosphorylations is illustrated (Figure S6B). Another indirect consequence of *wee* knockdown is the upregulation of Stat92E phosphorylation at Tyr711 in *wee*-deficient embryos (Table S5A). Cdk1 has been shown to regulate Stat92E phosphorylation at Tyr711 in cells (Baeg et al., 2005), and indeed, we detect elevated Y711-encompassing Stat92E phosphopeptides in *wee*-deficient embryos that cannot be attributed to increased Stat92E levels (Figure S5B).

Wee functions as a conserved tyrosine kinase (Campbell et al., 1995; McGowan and Russell, 1993); therefore, we inquired as to whether any phosphoproteins for which tyrosine phosphorylation was reduced in *wee*-deficient embryos are, in fact, direct Wee targets. We cloned and tagged eight genes for expression in *D. melanogaster* cells, which were selected based on reduced phosphorylation (>1.5-fold) of the corresponding protein in *wee*-deficient embryos. Of these, we observed hemagglutinin (HA)-tagged Wee in immunoprecipitates of FLAG-tagged Stonewall (Stwl: lane 6, Figure 7A). In the reciprocal direction, we detected FLAG-tagged Klp10A, CG13605, Stwl, and Polychaetoid (Pyd) in immunoprecipitates of HA-Wee (Figure S6D). Consistent with our observations, Pyd was previously identified in Wee-FLAG-HA immune complexes (Guruharsha et al., 2011).

We decided to focus on the nuclear protein Stwl, since the myb/SANT (Swi3, Ada2, N-CoR, TFIIB)-like domain it possesses has been found to influence histone modifications by modulating chromatin structure (Boyer et al., 2004) and *wee* mutant embryos have reported defects in chromatin condensation (Stumpff et al., 2004). Like other heterochromatin regulators, Stwl influences position effect variegation and HH3 methylation in vivo (Maines et al., 2007; Yi et al., 2009). We found that phosphopeptides encompassing Stwl Tyr305 were reduced in *wee*-deficient embryos (Figure 6F), despite total Stwl levels being elevated (lane 2 versus lane 1: Figure 7D). These alterations in protein cannot be attributed to mRNA transcript stability (Figure S6C). Based on our observations that *wee* is required for Stwl-Tyr305 phosphorylation, we examined the effects of *wee* overexpression on Tyr phosphorylation of Stwl in cells. Tyr phosphorylation of Stwl is elevated in cells overexpressing *wee*, based on phospho-Tyr immunoprecipitation and detection by immunoblotting (Figure 7B). To ask if Wee can directly phosphorylate Stwl, we generated His-tagged Stwl-fusion proteins for in vitro kinase assays. We incubated purified His-Stwl fragments with human WEE1 (38% identity, 53% similarity to *D. melanogaster* Wee). WEE1 phosphorylated Stwl at multiple sites recognized by a phospho-Tyr antibody, including fragments encompassing Tyr305 (Figure 7C, lanes 1 and 2). Interestingly, the BESS domain-containing fragment consistently inhibited WEE1 kinase activity, as indicated by reduced WEE1 autophosphorylation, both as a His-tagged protein (Figure 7C) and as a glutathione S-transferase (GST)-tagged fusion protein (data not shown). The BESS motif is likely the region that interacts with Wee, given that this domain facilitates protein-protein interactions (Bhaskar and Courey, 2002) and is often found together with the myb/SANT domain. The BESS motif of Suppressor of variegation 3-7 (Su(var)3-7) is required for its chromatin-silencing properties (Jaquet et al., 2006). Like Su(var)3-7, Stwl influences trimethylation of HH3 at Lys9, in addition to Lys27 at larval stages (Yi et al., 2009). We detected no obvious reduction in these repressive marks in *stwl*-depleted embryos. Rather, we observed alterations in trimethylated Lys4 of HH3, an activation mark (Figure 7E). Consistent with a role for Wee in inhibiting Stwl activity, HH3 trimethyl Lys4 marks are elevated in *wee*-deficient embryos (Figure 7E). Effects of *wee* knockdown on Lys4 methylation in later stage 2- to 4-hr embryos was confounded by the inability of *wee*-deficient embryos to transit the MBT (data not shown). Based on our observations, we propose that Wee inhibits the ability of Stwl to modulate histone methylation prior to the MBT, halting the activation of zygotic transcription to regulate the timing of transit through the MBT.

DISCUSSION

A Resource to Study Protein Kinases and Phosphatases in Early Embryos

We generated a validated collection of transgenic *D. melanogaster* shRNA lines targeting protein kinases and phosphatases maternally deposited in embryos. The collection permits the examination of zygotic lethal gene perturbations, without the effort of germline clone derivation. Multiple lines of evidence support that the embryonic phenotypes generated by our collection are, indeed, a result of shRNA on-targeting: (1) near-identical qualitative phenotypes generated by two unique shRNAs targeting the same gene for the 15% of the collection we tested; (2) abolition of shRNA-induced phenotypes by substitution of three nucleotides (C911s) precluding on-target binding; (3) the high degree of overlap between our shRNA-derived phenotypes and literature-reported mutant embryo and germline clone-derived embryo phenotypes; and (4) our general inability to accredit specific shRNA phenotypes to candidate OTEs derived from proteomics and partial complementarity matching.

A General Method to Predict Kinase Motifs and Targets

Using our shRNA collection, we performed quantitative phosphoproteome assessments of genetically compromised animals. An advantage of our gene knockdown strategy over gene knockout is that we restrict RNAi to the germline: since germline development is dispensable for organismal development, our RNAi method likely avoids major adaptation and compensation due to effects on the viability of the animal, such as that seen, for example, with yeast deletion mutants (Bodenmiller et al., 2010; Teng et al., 2013). Additionally, the modest amount of transcription in early-stage embryos further minimizes the possibility of compensation at the transcriptional level, although nontranscriptional compensation is a possibility. Conceivably, by comparing genetic knockout to incomplete depletion by RNAi-mediated knockdown, one could identify compensatory rewiring events. From phosphoproteomic profiling of kinase-deficient embryos, we identified altered phosphorylation of characterized substrates of depleted kinases and generated an extensive list of candidate substrates of the depleted kinase and altered phosphoproteins targeted by downstream kinases. A challenge will be to distinguish between primary and secondary targets. It is difficult to evaluate the number of primary targets per kinase since this will depend on multiple factors, including the function of the kinase and its expression level, localization, and connectivity with other proteins. Indeed, studies from yeast and mammalian kinases have illustrated that the number of substrates for any one kinase can range from hundreds to only a few (Ubersax and Ferrell, 2007). Thus, we expect variability in the number of substrates depending on the analyzed kinase. Furthermore, biologically meaningful alterations in phosphorylation may have been missed in our analyses, given the limitations of current mass spectrometry technology. We illustrate, however, that current instrumentation can be used to identify known and predicted targets relevant to the function of the perturbed kinase (e.g., Stwl is a direct target of Wee kinase) and so, despite perhaps only scratching the surface, we have generated biologically pertinent information. Additional information (e.g., in vitro kinase activity toward a substrate, protein-protein interaction, and functional assays) is necessary, of course, to infer a direct KS relationship (Sopko and Andrews, 2008). Undoubtedly, extension of our methodology will be effective for systematically mapping substrates to culpable kinases and for pinpointing critical phosphosites important for substrate function.

Correlation and Anticorrelation: An Application for Network Analysis

Our correlative analysis examining coordination between alterations in phosphosite pairs among kinase-deficient profiles

uncovered signaling mechanisms. We demonstrate how a role for Slik kinase in regulating the transcription factor Stat92E could be predicted from correlative phosphorylation of these two proteins. The predictive power of this approach could be extended by knowing if specific phosphorylation events serve activating or inhibitory functions and by superimposing kinase consensus motifs. Our analysis demonstrates how functional phosphorylation might be uncovered in any phosphoproteomic data using simple correlative principles. Notably, predictions for any particular kinase can be made indirectly from its detection in varying genetic contexts, with no requirement for direct modulation of the queried kinase. The data we generated from embryos will complement orthogonal data sets such as kinase consensus motif and protein-protein interaction data derived from, for example, peptide and protein chip assays, coaffinity purifications, and yeast two-hybrid assays. Furthermore, phosphosite correlation information could be integrated with large-scale RNAi phenotype data in order to predict whether phosphorylation of a target by a specific kinase serves an activating or inhibiting function.

Perspective

Given that key signaling pathways and kinases implicated in human disease are conserved in *Drosophila* (Rubin et al., 2000), the insight gained from our kinase-deficient phosphoproteomic signatures constitutes an important step toward understanding the kinome network. Going forward, we anticipate that phosphoproteomic assessment of other posttranslational modifications and more complex genotypes, using combinatorial knockdown (two shRNAs) or knockdown in combination with transgene overexpression or gain-of-function mutations, will appreciably illuminate our ability to decipher signaling mechanisms. In this way, global proteomic analyses could map pathways but also reveal critical nodes in signaling that may partially or completely overcome mutations resulting in pathway hyperactivity. Alternatively, phosphoproteomic assessment of a sensitized kinase mutant in the context of a substrate gain of function could expose altered signaling mechanisms contributing to compromised viability (Sopko et al., 2006). Finally, genetic combinations would mimic more natural scenarios in terms of genetic heterogeneity contributing to susceptibility to disease and, by mapping contextual phosphorylation, would improve on our ability to predict and target essential signaling nodes.

EXPERIMENTAL PROCEDURES

Detailed methods are available in the Supplemental Experimental Procedures. Mass spectrometric sample preparation is further described in the Protocol.

Transgenic shRNA Line Generation

shRNAs (21 base pairs) were cloned into VALIUM series vectors and injected into embryos for targeted phiC31-mediated integration at genomic attP landing sites on the second or third chromosome as described elsewhere (Ni et al., 2011). All transgenic lines were sequenced to confirm the identity of the shRNA and miR-1 scaffold.

Protein Kinase or Phosphatase-Deficient Embryo Derivation

Females heterozygous for the UAS-shRNA and either MTD-Gal4 (Petrella et al., 2007), expressing three versions of Gal4 sequentially throughout oogenesis, or tub-Gal4, a line expressing Gal4 from a maternal tubulin promoter at two insertion sites during mid- and late oogenesis (Staller et al., 2013), were crossed to UAS-shRNA males to recover fertilized embryos.

RNA Isolation, Reverse Transcription, and Real-Time qPCR

RNA was isolated by guanidinium thiocyanate-phenol-chloroform extraction using TRIzol (Life Technologies) and glass-bead-based cell disruption. Genomic DNA was eliminated by incubation with DNase (QIAGEN), and samples were processed for cleanup with an RNeasy MinElute Cleanup Kit (QIAGEN).

One microgram of purified RNA was incubated with a mix of oligo(dT) and random hexamer primers and with iScript RT (iScript cDNA Synthesis Kit, Bio-Rad) for complementary DNA (cDNA) synthesis. cDNA was used as the template for amplification, using validated primers in iQ SYBR Green Supermix with a CFX96 Real-Time PCR detection system (Bio-Rad). Query gene expression was relative to a control sample, normalized to the expression of three reference genes: *ribosomal protein L32*, *alpha-tubulin*, and either *nuclear fallout* or *Gapdh1*, using the $\Delta\Delta C(t)$ analysis method.

Maternal Phenotype Derivation

Hatch rate was calculated from counting embryos 24 hr after deposition. For genotypes with defective hatching, cuticles prepared in Hoyer's mounting media were imaged with a Zeiss AxioCam HRC Camera mounted on a Zeiss Axiophot microscope.

Coimmunoprecipitation and Immunoblotting

Lysates were subjected to immunoprecipitation using the indicated antibodies, and samples were subjected to SDS-PAGE followed by immunoblotting.

Quantitative Phosphoproteomics

Embryos lysed in 8 M urea were digested with trypsin, and peptides were chemically labeled with one of six TMT Isobaric Mass Tags (Thermo Fisher Scientific), separated into 12 fractions by strong cation exchange chromatography, purified with TiO_2 microspheres, and analyzed via liquid chromatography-tandem mass spectrometry on an Orbitrap Velos Pro mass spectrometer (Thermo Fisher Scientific). Peptides were identified by Sequest and filtered to a 1% peptide false discovery rate (FDR). Proteins were filtered to achieve a 2% final protein FDR (final peptide FDR near 0.15%). TMT reporter ion intensities for individual phosphopeptides were normalized to the summed reporter ion intensity for each TMT label. The localizations of phosphorylations were assigned using the AScore algorithm.

In Vitro Kinase Assay

In vitro kinase assays were carried out as described elsewhere (Sopko et al., 2006).

Correlative Analysis

A phosphosite matrix was constructed where rows correspond to identified phosphosites and columns correspond to kinase-deficient data sets. Only phosphosites with ≥ 0.58 $\log_2$-fold change were distinguished, by values +1 and −1, based on an increase or decrease, respectively, in levels relative to an shRNA control. All pairwise combinations of phosphosites were classified as positive or negative correlating based on their change in the same or opposite direction, respectively, for each kinase-deficient condition. A correlation sign score was determined, considering the number of positive and negative correlations and the total number of kinase-deficient phosphorylation profiles where both phosphosites change.

SUPPLEMENTAL INFORMATION

Supplemental Information includes Supplemental Experimental Procedures, six figures, seven tables, and a Protocol and can be found with this article online at http://dx.doi.org/10.1016/j.devcel.2014.07.027.

ACKNOWLEDGMENTS

We thank S. Campbell, D. McKearin, and T.T. Su for flies and antibodies. We thank the Transgenic RNAi Project (TRiP) at Harvard Medical School for flies,

specifically R. Tao for shRNA plasmid construction; C. Villalta and P. Namgyal for injections; C. Kelley for help with sequencing; A. Housden and A. Miller for help with stock establishment; and L. Holderbaum for TRiP database management. We additionally thank the Bloomington Drosophila Stock Center for flies, the Developmental Studies Hybridoma Bank for antibodies, and the Drosophila RNAi Screening Center (Harvard Medical School), particularly Q. Gilly and I. Flockhart for dsRNA amplicons, equipment, and database assistance. We thank H. Kuhn, W. Kim, S. Mohr, and X. Varelas for critical comments on the manuscript. We thank the N.P. and S.P.G. labs for helpful suggestions and advice, in particular E. Huttlin. The NIH supported this work (5R01DK088718, 5P01CA120964, 5R01GM084947, and 5R01GM067761). R.S. is a Special Fellow of the Leukemia and Lymphoma Society. N.P. is a Howard Hughes Medical Institute investigator.

Received: February 28, 2014
Revised: June 24, 2014
Accepted: July 28, 2014
Published: October 2, 2014

REFERENCES

Adams, R.R., Maiato, H., Earnshaw, W.C., and Carmena, M. (2001). Essential roles of Drosophila inner centromere protein (INCENP) and aurora B in histone H3 phosphorylation, metaphase chromosome alignment, kinetochore disjunction, and chromosome segregation. J. Cell Biol. *153*, 865–880.

Alexander, J., Lim, D., Joughin, B.A., Hegemann, B., Hutchins, J.R., Ehrenberger, T., Ivins, F., Sessa, F., Hudecz, O., Nigg, E.A., et al. (2011). Spatial exclusivity combined with positive and negative selection of phosphorylation motifs is the basis for context-dependent mitotic signaling. Sci. Signal. *4*, ra42.

Baeg, G.H., Zhou, R., and Perrimon, N. (2005). Genome-wide RNAi analysis of JAK/STAT signaling components in Drosophila. Genes Dev. *19*, 1861–1870.

Bhaskar, V., and Courey, A.J. (2002). The MADF-BESS domain factor Dip3 potentiates synergistic activation by Dorsal and Twist. Gene *299*, 173–184.

Bodenmiller, B., Wanka, S., Kraft, C., Urban, J., Campbell, D., Pedrioli, P.G., Gerrits, B., Picotti, P., Lam, H., Vitek, O., et al. (2010). Phosphoproteomic analysis reveals interconnected system-wide responses to perturbations of kinases and phosphatases in yeast. Sci. Signal. *3*, rs4.

Boyer, L.A., Latek, R.R., and Peterson, C.L. (2004). The SANT domain: a unique histone-tail-binding module? Nat. Rev. Mol. Cell Biol. *5*, 158–163.

Brand, A.H., and Perrimon, N. (1993). Targeted gene expression as a means of altering cell fates and generating dominant phenotypes. Development *118*, 401–415.

Buehler, E., Chen, Y.C., and Martin, S. (2012). C911: A bench-level control for sequence specific siRNA off-target effects. PLoS ONE *7*, e51942.

Bustin, S.A., Benes, V., Garson, J.A., Hellemans, J., Huggett, J., Kubista, M., Mueller, R., Nolan, T., Pfaffl, M.W., Shipley, G.L., et al. (2009). The MIQE guidelines: minimum information for publication of quantitative real-time PCR experiments. Clin. Chem. *55*, 611–622.

Campbell, S.D., Sprenger, F., Edgar, B.A., and O'Farrell, P.H. (1995). Drosophila Wee1 kinase rescues fission yeast from mitotic catastrophe and phosphorylates Drosophila Cdc2 in vitro. Mol. Biol. Cell *6*, 1333–1347.

Chou, T.B., and Perrimon, N. (1996). The autosomal FLP-DFS technique for generating germline mosaics in Drosophila melanogaster. Genetics *144*, 1673–1679.

Chou, M.F., and Schwartz, D. (2011). Biological sequence motif discovery using motif-x. Curr. Protoc. Bioinformatics *Chapter 13*, Unit 13, 15–24.

Davidson, G., Wu, W., Shen, J., Bilic, J., Fenger, U., Stannek, P., Glinka, A., and Niehrs, C. (2005). Casein kinase 1 gamma couples Wnt receptor activation to cytoplasmic signal transduction. Nature *438*, 867–872.

Glatter, T., Schittenhelm, R.B., Rinner, O., Roguska, K., Wepf, A., Jünger, M.A., Köhler, K., Jevtov, I., Choi, H., Schmidt, A., et al. (2011). Modularity and hormone sensitivity of the Drosophila melanogaster insulin receptor/target of rapamycin interaction proteome. Mol. Syst. Biol. *7*, 547.

Gnad, F., Forner, F., Zielinska, D.F., Birney, E., Gunawardena, J., and Mann, M. (2010). Evolutionary constraints of phosphorylation in eukaryotes, prokaryotes, and mitochondria. Mol. Cell. Proteomics *9*, 2642–2653.

Graveley, B.R., Brooks, A.N., Carlson, J.W., Duff, M.O., Landolin, J.M., Yang, L., Artieri, C.G., van Baren, M.J., Boley, N., Booth, B.W., et al. (2011). The developmental transcriptome of Drosophila melanogaster. Nature *471*, 473–479.

Guruharsha, K.G., Rual, J.F., Zhai, B., Mintseris, J., Vaidya, P., Vaidya, N., Beekman, C., Wong, C., Rhee, D.Y., Cenaj, O., et al. (2011). A protein complex network of Drosophila melanogaster. Cell *147*, 690–703.

Hipfner, D.R., and Cohen, S.M. (2003). The Drosophila sterile-20 kinase slik controls cell proliferation and apoptosis during imaginal disc development. PLoS Biol. *1*, E35.

Holt, L.J., Tuch, B.B., Villén, J., Johnson, A.D., Gygi, S.P., and Morgan, D.O. (2009). Global analysis of Cdk1 substrate phosphorylation sites provides insights into evolution. Science *325*, 1682–1686.

Hu, Y., Flockhart, I., Vinayagam, A., Bergwitz, C., Berger, B., Perrimon, N., and Mohr, S.E. (2011). An integrative approach to ortholog prediction for disease-focused and other functional studies. BMC Bioinformatics *12*, 357.

Hu, Y., Roesel, C., Flockhart, I., Perkins, L., Perrimon, N., and Mohr, S.E. (2013a). UP-TORR: online tool for accurate and Up-to-Date annotation of RNAi Reagents. Genetics *195*, 37–45.

Hu, Y., Sopko, R., Foos, M., Kelley, C., Flockhart, I., Ammeux, N., Wang, X., Perkins, L., Perrimon, N., and Mohr, S.E. (2013b). FlyPrimerBank: an online database for Drosophila melanogaster gene expression analysis and knockdown evaluation of RNAi reagents. G3 (Bethesda) *3*, 1607–1616.

Hummel, T., Attix, S., Gunning, D., and Zipursky, S.L. (2002). Temporal control of glial cell migration in the Drosophila eye requires gilgamesh, hedgehog, and eye specification genes. Neuron *33*, 193–203.

Jang, C.Y., Coppinger, J.A., Seki, A., Yates, J.R., 3rd, and Fang, G. (2009). Plk1 and Aurora A regulate the depolymerase activity and the cellular localization of Kif2a. J. Cell Sci. *122*, 1334–1341.

Jaquet, Y., Delattre, M., Montoya-Burgos, J., Spierer, A., and Spierer, P. (2006). Conserved domains control heterochromatin localization and silencing properties of SU(VAR)3-7. Chromosoma *115*, 139–150.

Kang, J., Cheeseman, I.M., Kallstrom, G., Velmurugan, S., Barnes, G., and Chan, C.S. (2001). Functional cooperation of Dam1, Ipl1, and the inner centromere protein (INCENP)-related protein Sli15 during chromosome segregation. J. Cell Biol. *155*, 763–774.

Landry, C.R., Levy, E.D., and Michnick, S.W. (2009). Weak functional constraints on phosphoproteomes. Trends Genet. *25*, 193–197.

Maines, J.Z., Park, J.K., Williams, M., and McKearin, D.M. (2007). Stonewalling Drosophila stem cell differentiation by epigenetic controls. Development *134*, 1471–1479.

Manning, G., Whyte, D.B., Martinez, R., Hunter, T., and Sudarsanam, S. (2002). The protein kinase complement of the human genome. Science *298*, 1912–1934.

Marguerat, S., Schmidt, A., Codlin, S., Chen, W., Aebersold, R., and Bähler, J. (2012). Quantitative analysis of fission yeast transcriptomes and proteomes in proliferating and quiescent cells. Cell *151*, 671–683.

McGowan, C.H., and Russell, P. (1993). Human Wee1 kinase inhibits cell division by phosphorylating p34cdc2 exclusively on Tyr15. EMBO J. *12*, 75–85.

Miller, M.L., Jensen, L.J., Diella, F., Jørgensen, C., Tinti, M., Li, L., Hsiung, M., Parker, S.A., Bordeaux, J., Sicheritz-Ponten, T., et al. (2008). Linear motif atlas for phosphorylation-dependent signaling. Sci. Signal. *1*, ra2.

Morrison, D.K., Murakami, M.S., and Cleghon, V. (2000). Protein kinases and phosphatases in the Drosophila genome. J. Cell Biol. *150*, F57–F62.

Ni, J.Q., Zhou, R., Czech, B., Liu, L.P., Holderbaum, L., Yang-Zhou, D., Shim, H.S., Tao, R., Handler, D., Karpowicz, P., et al. (2011). A genome-scale shRNA resource for transgenic RNAi in Drosophila. Nat. Methods *8*, 405–407.

Perrimon, N., Ni, J.Q., and Perkins, L. (2010). In vivo RNAi: today and tomorrow. Cold Spring Harb. Perspect. Biol. *2*, a003640.

Petrella, L.N., Smith-Leiker, T., and Cooley, L. (2007). The Ovhts polyprotein is cleaved to produce fusome and ring canal proteins required for Drosophila oogenesis. Development *134*, 703–712.

Price, D., Rabinovitch, S., O'Farrell, P.H., and Campbell, S.D. (2000). Drosophila wee1 has an essential role in the nuclear divisions of early embryogenesis. Genetics *155*, 159–166.

Rubin, G.M., Yandell, M.D., Wortman, J.R., Gabor Miklos, G.L., Nelson, C.R., Hariharan, I.K., Fortini, M.E., Li, P.W., Apweiler, R., Fleischmann, W., et al. (2000). Comparative genomics of the eukaryotes. Science *287*, 2204–2215.

Sawka-Verhelle, D., Filloux, C., Tartare-Deckert, S., Mothe, I., and Van Obberghen, E. (1997). Identification of Stat 5B as a substrate of the insulin receptor. Eur. J. Biochem. *250*, 411–417.

Sharifpoor, S., Nguyen Ba, A.N., Youn, J.Y., van Dyk, D., Friesen, H., Douglas, A.C., Kurat, C.F., Chong, Y.T., Founk, K., Moses, A.M., and Andrews, B.J. (2011). A quantitative literature-curated gold standard for kinase-substrate pairs. Genome Biol. *12*, R39.

Sopko, R., and Andrews, B.J. (2008). Linking the kinome and phosphorylome—a comprehensive review of approaches to find kinase targets. Mol. Biosyst. *4*, 920–933.

Sopko, R., Huang, D., Preston, N., Chua, G., Papp, B., Kafadar, K., Snyder, M., Oliver, S.G., Cyert, M., Hughes, T.R., et al. (2006). Mapping pathways and phenotypes by systematic gene overexpression. Mol. Cell *21*, 319–330.

Staller, M.V., Yan, D., Randklev, S., Bragdon, M.D., Wunderlich, Z.B., Tao, R., Perkins, L.A., Depace, A.H., and Perrimon, N. (2013). Depleting gene activities in early Drosophila embryos with the "maternal-Gal4-shRNA" system. Genetics *193*, 51–61.

Stumpff, J., Duncan, T., Homola, E., Campbell, S.D., and Su, T.T. (2004). Drosophila Wee1 kinase regulates Cdk1 and mitotic entry during embryogenesis. Curr. Biol. *14*, 2143–2148.

Szilagyi, Z., and Gustafsson, C.M. (2013). Emerging roles of Cdk8 in cell cycle control. Biochim. Biophys. Acta *1829*, 916–920.

Teng, X., Dayhoff-Brannigan, M., Cheng, W.C., Gilbert, C.E., Sing, C.N., Diny, N.L., Wheelan, S.J., Dunham, M.J., Boeke, J.D., Pineda, F.J., and Hardwick, J.M. (2013). Genome-wide consequences of deleting any single gene. Mol. Cell *52*, 485–494.

Ubersax, J.A., and Ferrell, J.E., Jr. (2007). Mechanisms of specificity in protein phosphorylation. Nat. Rev. Mol. Cell Biol. *8*, 530–541.

Wu, R., Dephoure, N., Haas, W., Huttlin, E.L., Zhai, B., Sowa, M.E., and Gygi, S.P. (2011). Correct interpretation of comprehensive phosphorylation dynamics requires normalization by protein expression changes. Mol. Cell Proteomics *10*, M111.009654.

Yan, R., Small, S., Desplan, C., Dearolf, C.R., and Darnell, J.E., Jr. (1996). Identification of a Stat gene that functions in Drosophila development. Cell *84*, 421–430.

Yan, D., Neumüller, R.A., Buckner, M., Ayers, K., Li, H., Hu, Y., Yang-Zhou, D., Pan, L., Wang, X., Kelley, C., et al. (2014). A regulatory network of Drosophila germline stem cell self-renewal. Dev. Cell *28*, 459–473.

Yi, X., de Vries, H.I., Siudeja, K., Rana, A., Lemstra, W., Brunsting, J.F., Kok, R.M., Smulders, Y.M., Schaefer, M., Dijk, F., et al. (2009). Stwl modifies chromatin compaction and is required to maintain DNA integrity in the presence of perturbed DNA replication. Mol. Biol. Cell *20*, 983–994.

Zhang, Y., Liu, Y., Li, X., Gao, W., Zhang, W., Guan, Q., Jiang, J., Frank, S.J., and Wang, X. (2013). Effects of insulin and IGF-I on growth hormone- induced STAT5 activation in 3T3-F442A adipocytes. Lipids Health Dis. *12*, 56.

Developmental Cell, Volume *31*

Supplemental Information

Combining Genetic Perturbations and Proteomics to Examine Kinase-Phosphatase Networks in *Drosophila* Embryos

Richelle Sopko, Marianna Foos, Arunachalam Vinayagam, Bo Zhai, Richard Binari, Yanhui Hu, Sakara Randklev, Lizabeth A. Perkins, Steven P. Gygi, and Norbert Perrimon

Figure S1

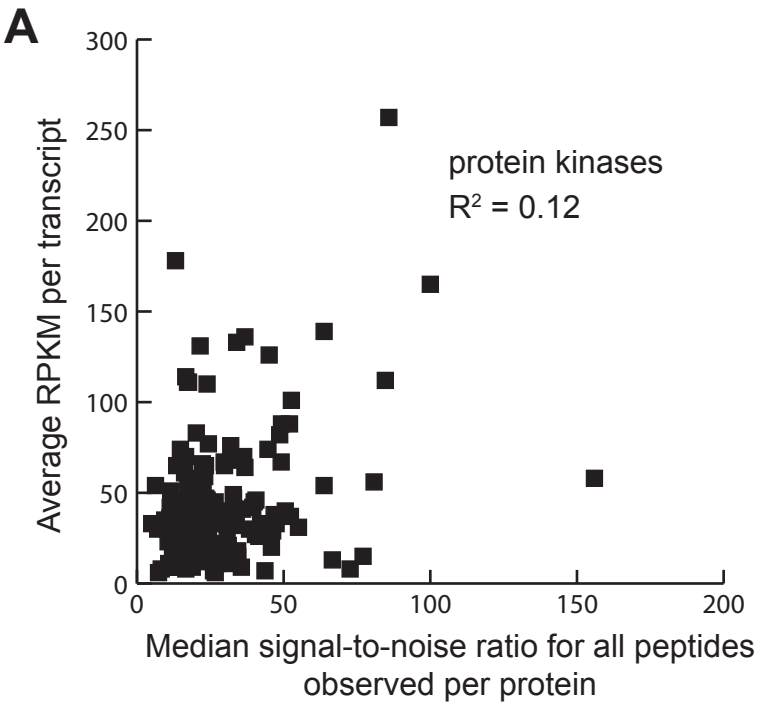
A
300
250
200
150
100
50
0
Average RPKM per transcript
protein kinases
R² = 0.12
0
50
100
150
200
Median signal-to-noise ratio for all peptides observed per protein

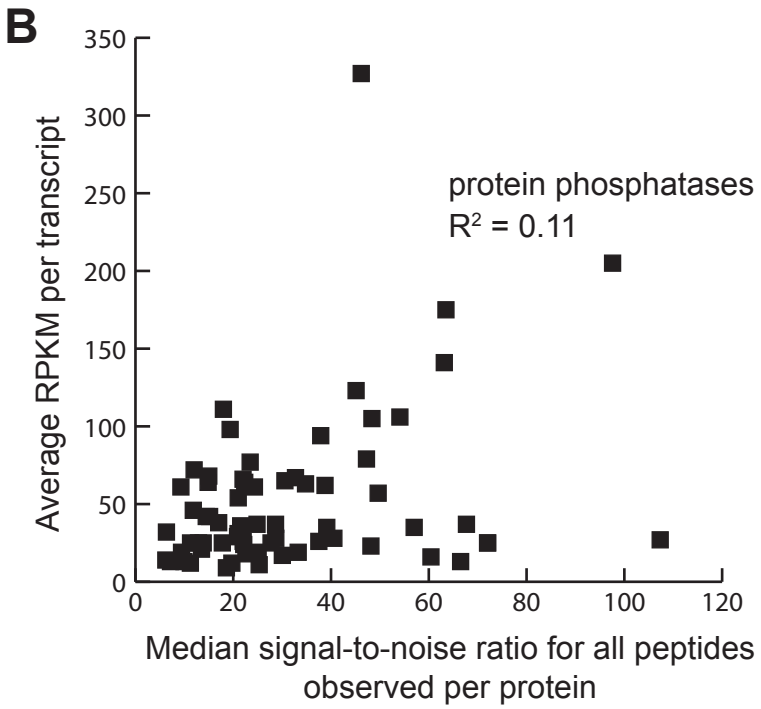
B
350
300
250
200
150
100
50
0
Average RPKM per transcript
protein phosphatases
R² = 0.11
0
20
40
60
80
100
120
Median signal-to-noise ratio for all peptides observed per protein

Figure S2

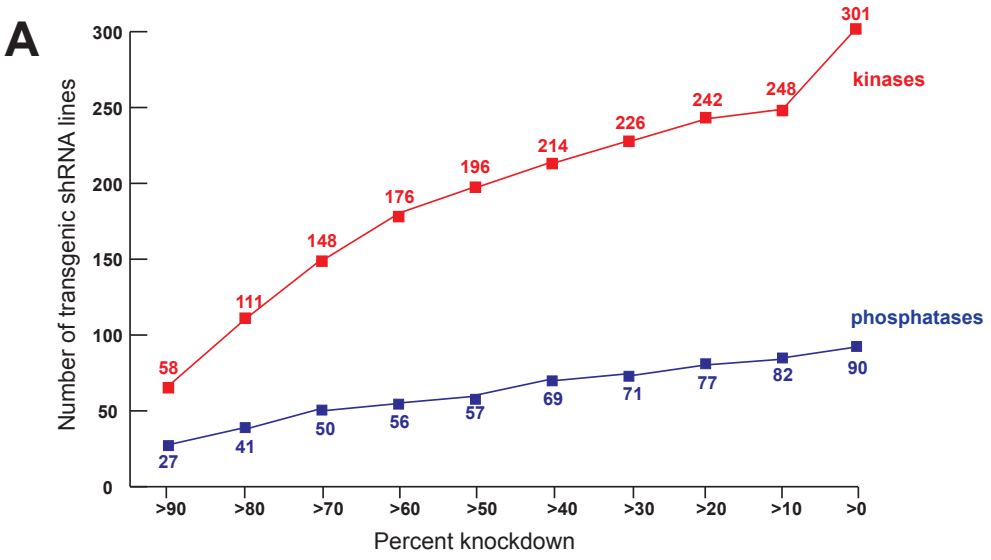
A
Number of transgenic shRNA lines
Percent knockdown
kinases
phosphatases
301
248
242
226
214
196
176
148
111
58
90
82
77
71
69
57
56
50
41
27
>90
>80
>70
>60
>50
>40
>30
>20
>10
>0

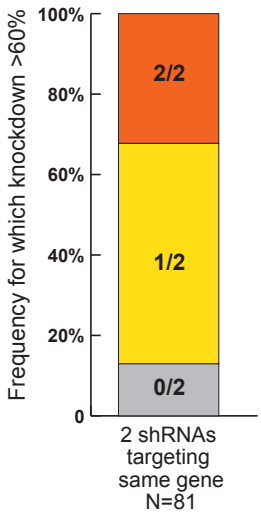
B
Frequency for which knockdown >60%
2/2
1/2
0/2
2 shRNAs targeting same gene N=81

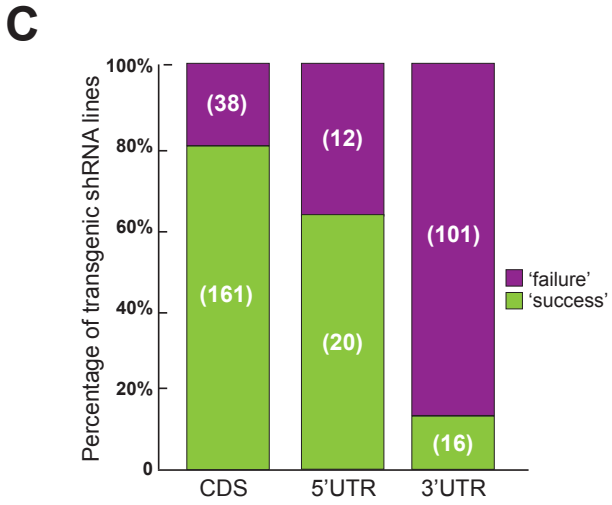
C
Percentage of transgenic shRNA lines
(38)
(161)
(12)
(20)
(101)
(16)
'failure'
'success'
CDS
5'UTR
3'UTR

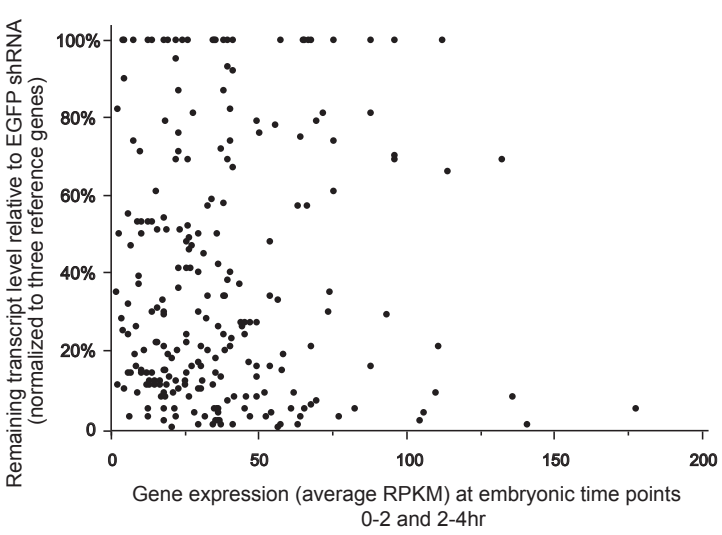
D
Remaining transcript level relative to EGFP shRNA (normalized to three reference genes)
Gene expression (average RPKM) at embryonic time points 0-2 and 2-4hr

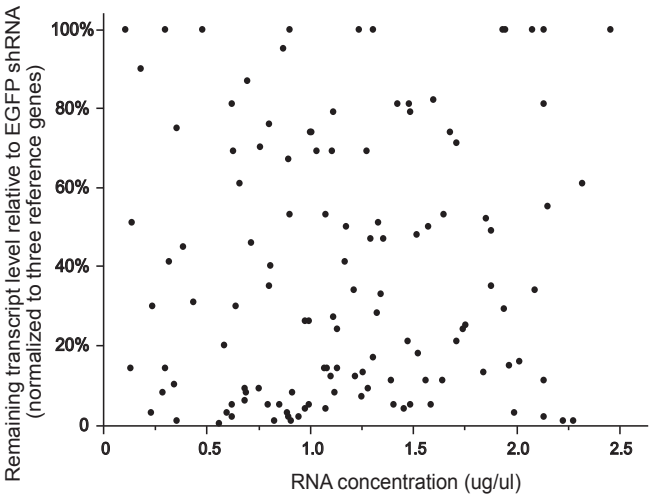
E
Remaining transcript level relative to EGFP shRNA (normalized to three reference genes)
RNA concentration (ug/ul)

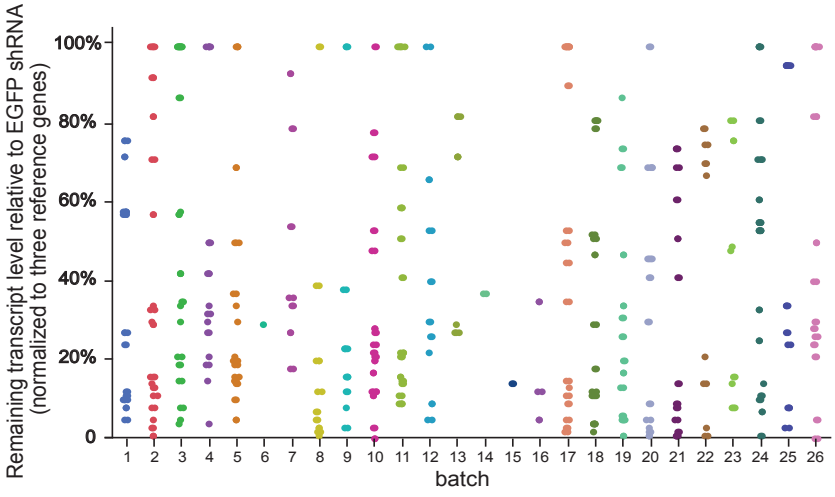
F
Remaining transcript level relative to EGFP shRNA (normalized to three reference genes)
batch

Figure S3

A Reporter Ion Abundance Between Replicates

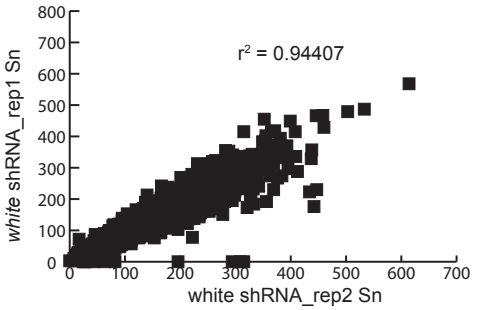

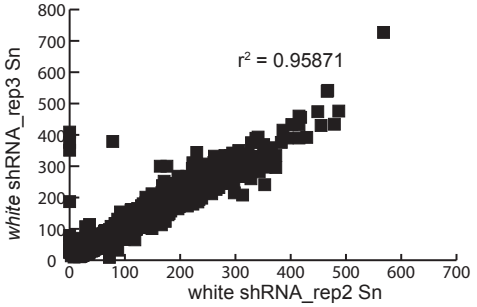

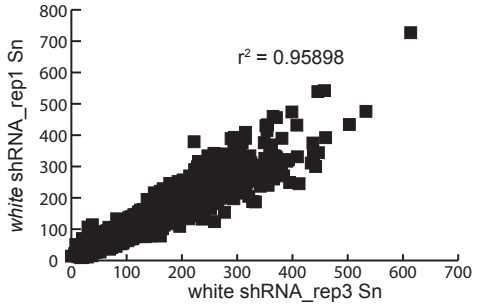

Phosphopeptide Identity Between Replicates

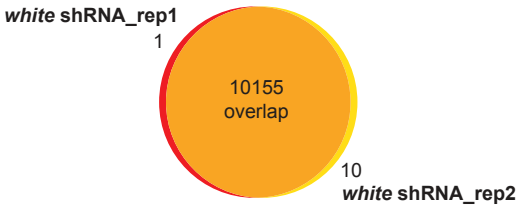

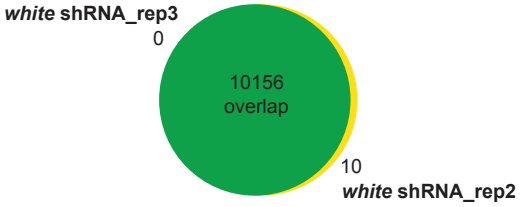

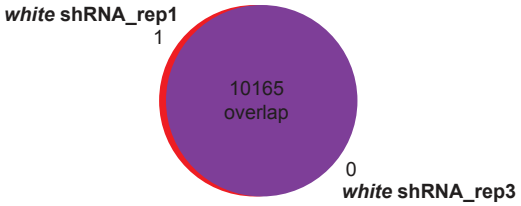

B Reporter Ion Abundance Between Replicates

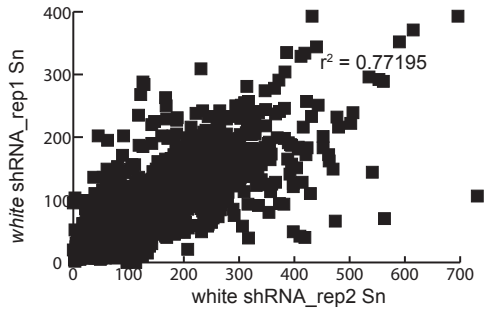

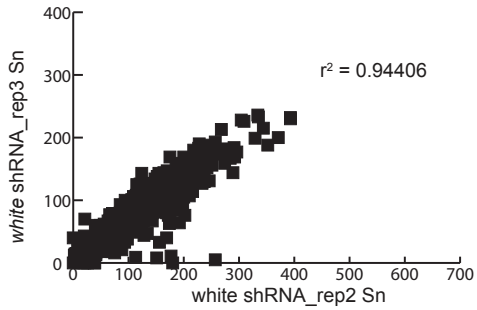

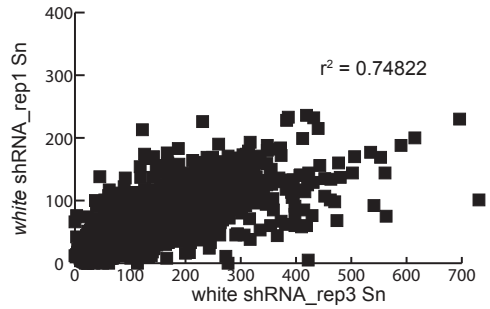

Phosphopeptide Identity Between Replicates

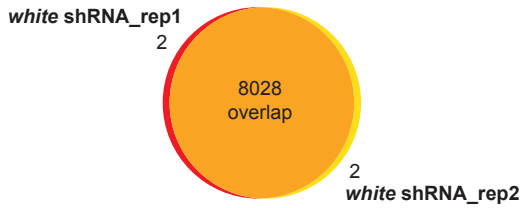

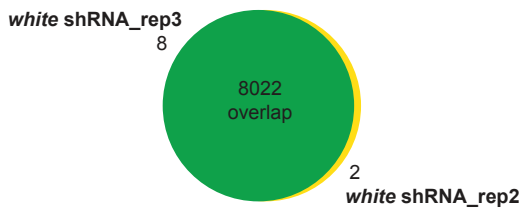

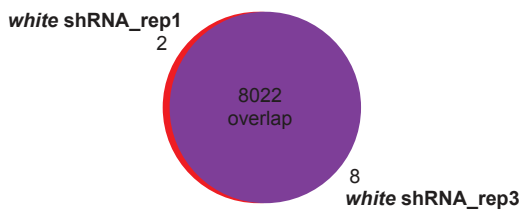

Figure S4

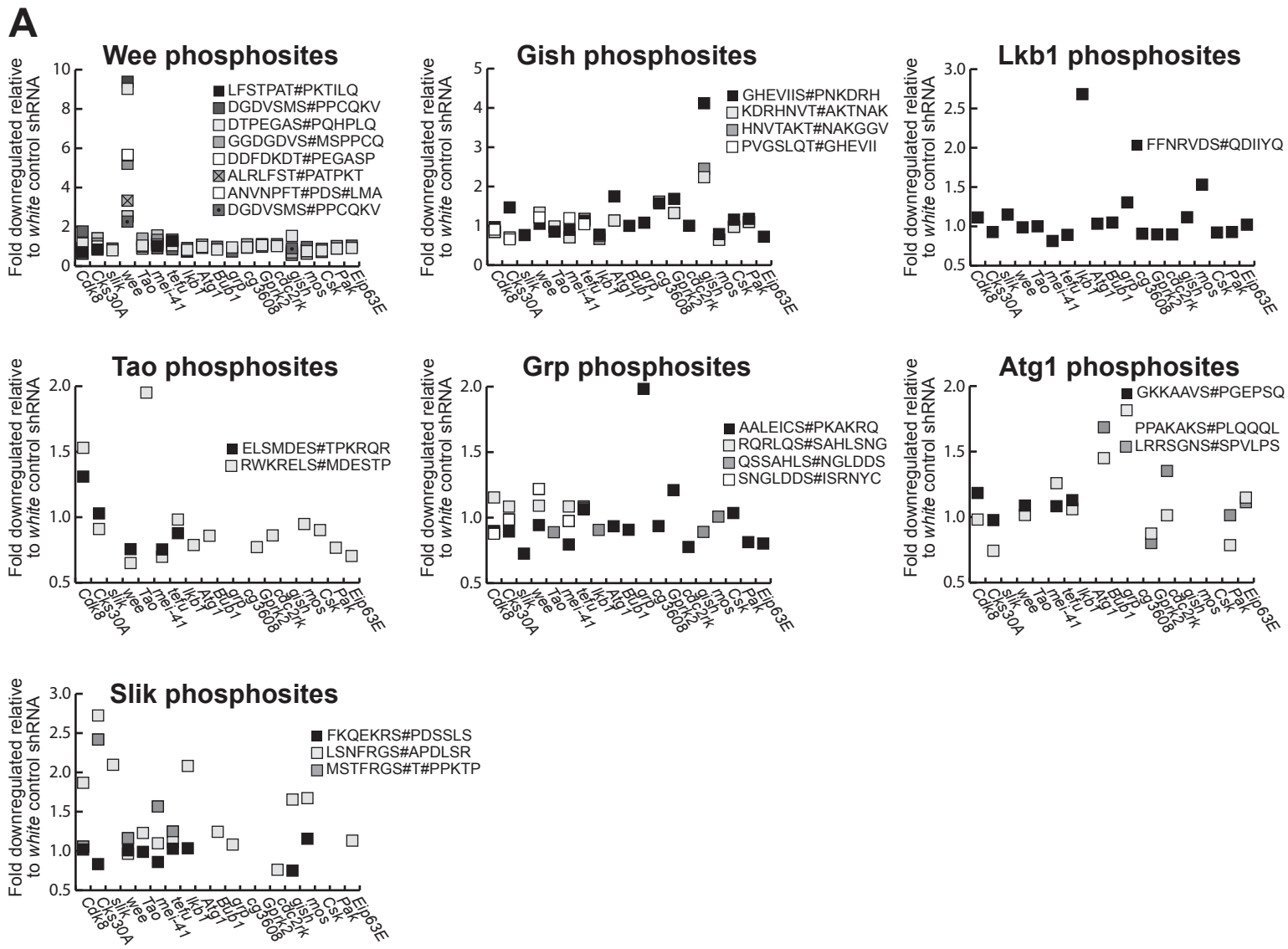
A
Wee phosphosites
LFSTPAT#PKTILQ
DGDVSMS#PPCQKV
DTPEGAS#PQHPLQ
GGDGDVS#MSPPCQ
DDFDKDT#PEGASP
ALRLFST#PATPKT
ANVNPFT#PDS#LMA
DGDVSMS#PPCQKV
Gish phosphosites
GHEVIIS#PNKDRH
KDRHNVT#AKTNAK
HNVTAKT#NAKGGV
PVGSLQT#GHEVII
Lkb1 phosphosites
FFNRVDS#QDIIYQ
Tao phosphosites
ELSMDES#TPKRQR
RWKRELS#MDESTP
Grp phosphosites
AALEICS#PKAKRQ
RQRLQS#SAHLSNG
QSSAHLS#NGLDDS
SNGLDDS#ISRNYC
Atg1 phosphosites
GKKAAVS#PGEPSQ
PPAKAKS#PLQQQL
LRRSGNS#SPVLPS
Slik phosphosites
FKQEKRS#PDSSLS
LSNFRGS#APDLSR
MSTFRGS#T#PPKTP
Fold downregulated relative to white control shRNA
Cdk8
Cks30A
slik
wee
Tao
mei-41
tefu
lkb1
Atg1
Bub1
grp
cg3608
Gprk2
cdc2rk
gish
mos
Csk
Pak
Eip63E

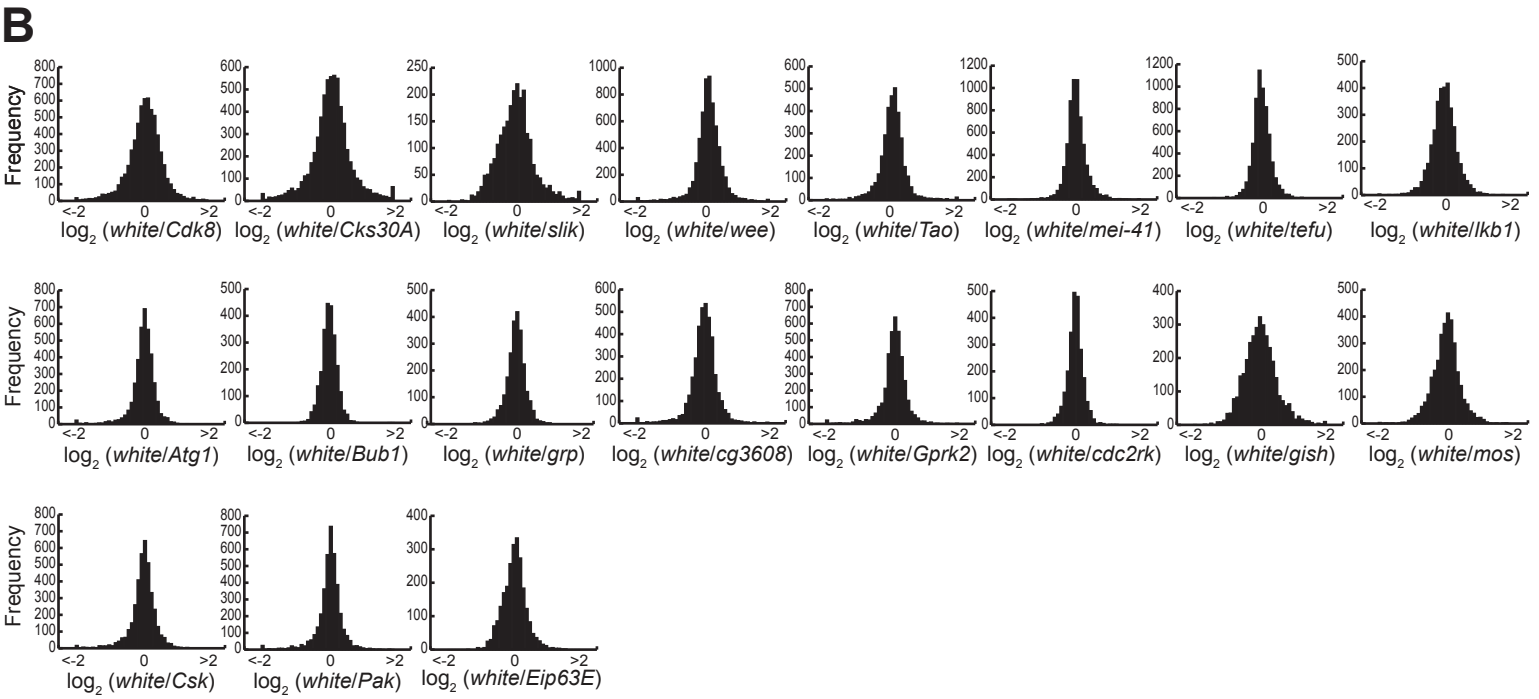
B
Frequency
log2 (white/Cdk8)
log2 (white/Cks30A)
log2 (white/slik)
log2 (white/wee)
log2 (white/Tao)
log2 (white/mei-41)
log2 (white/tefu)
log2 (white/lkb1)
log2 (white/Atg1)
log2 (white/Bub1)
log2 (white/grp)
log2 (white/cg3608)
log2 (white/Gprk2)
log2 (white/cdc2rk)
log2 (white/gish)
log2 (white/mos)
log2 (white/Csk)
log2 (white/Pak)
log2 (white/Eip63E)

Figure S5

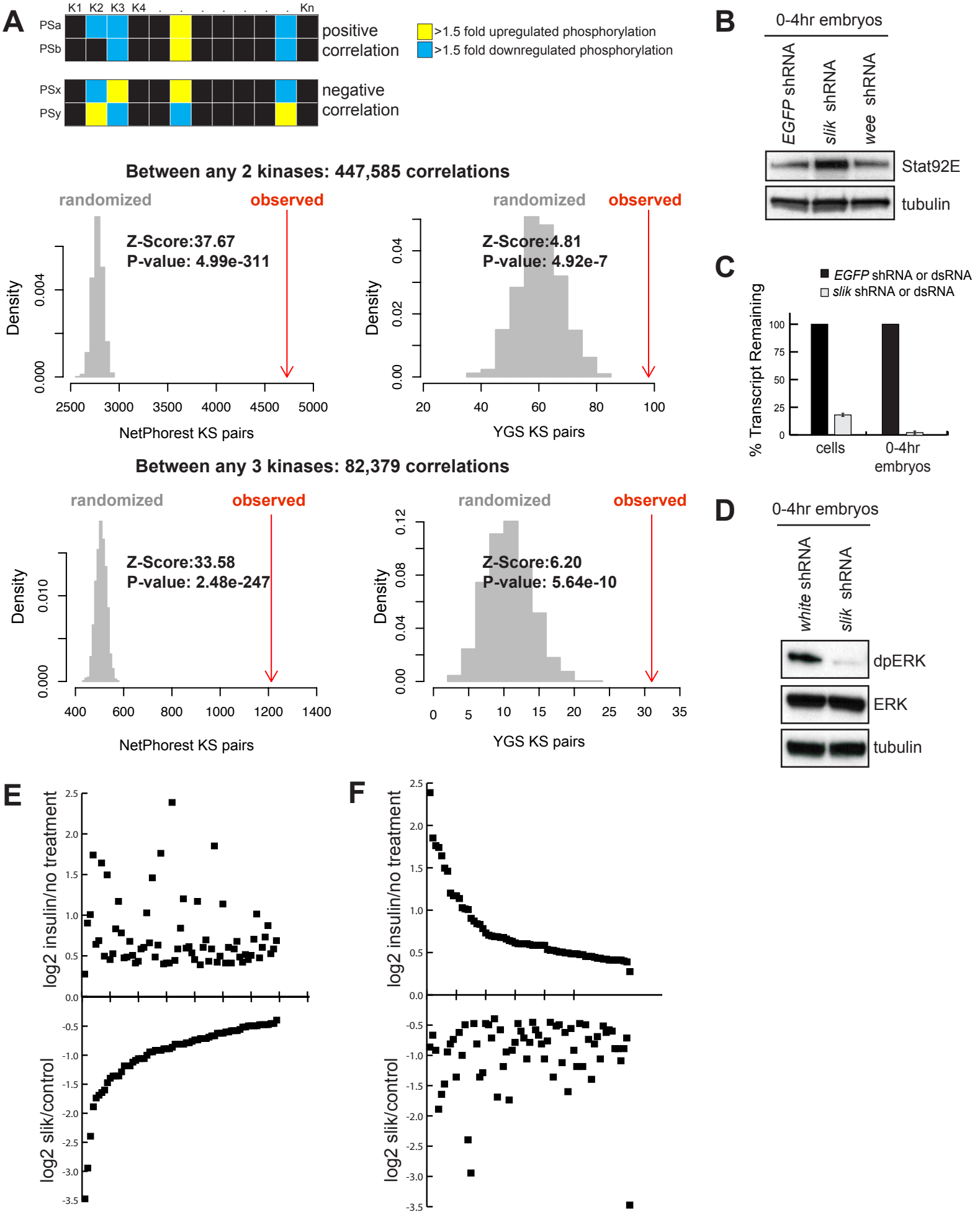
A
K1 K2 K3 K4 . . . . . Kn
PSa
PSb
positive correlation
PSx
PSy
negative correlation
>1.5 fold upregulated phosphorylation
>1.5 fold downregulated phosphorylation
Between any 2 kinases: 447,585 correlations
randomized
observed
Z-Score:37.67
P-value: 4.99e-311
Density
NetPhorest KS pairs
Z-Score:4.81
P-value: 4.92e-7
YGS KS pairs
Between any 3 kinases: 82,379 correlations
Z-Score:33.58
P-value: 2.48e-247
Z-Score:6.20
P-value: 5.64e-10
B
0-4hr embryos
EGFP shRNA
slik shRNA
wee shRNA
Stat92E
tubulin
C
EGFP shRNA or dsRNA
slik shRNA or dsRNA
% Transcript Remaining
cells
0-4hr embryos
D
0-4hr embryos
white shRNA
slik shRNA
dpERK
ERK
tubulin
E
log2 insulin/no treatment
log2 slik/control
F
log2 insulin/no treatment
log2 slik/control

Figure S6

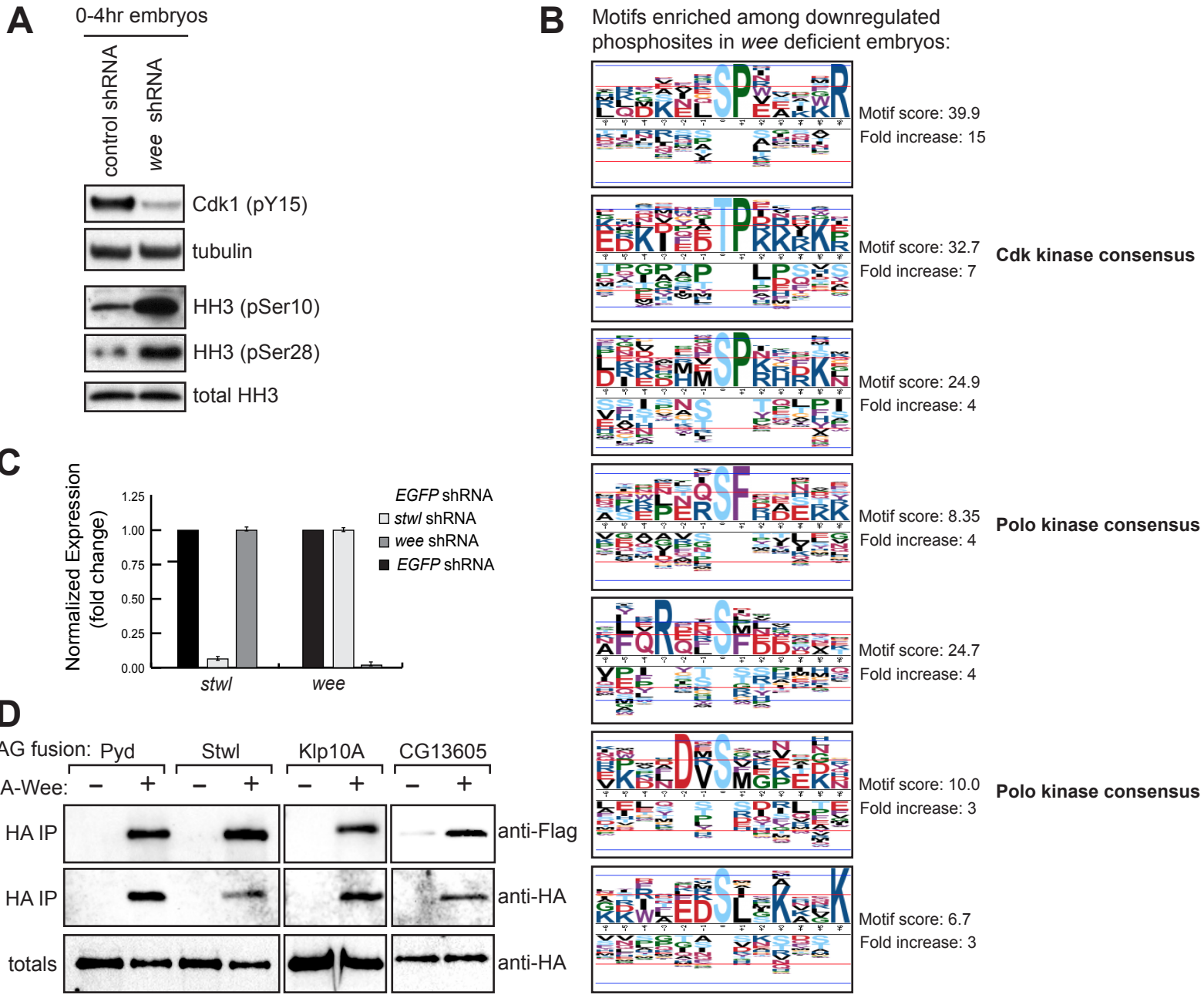
A
0-4hr embryos
control shRNA
wee shRNA
Cdk1 (pY15)
tubulin
HH3 (pSer10)
HH3 (pSer28)
total HH3
B
Motifs enriched among downregulated phosphosites in wee deficient embryos:
Motif score: 39.9
Fold increase: 15
Motif score: 32.7
Fold increase: 7
Cdk kinase consensus
Motif score: 24.9
Fold increase: 4
Motif score: 8.35
Fold increase: 4
Polo kinase consensus
Motif score: 24.7
Fold increase: 4
Motif score: 10.0
Fold increase: 3
Polo kinase consensus
Motif score: 6.7
Fold increase: 3
C
Normalized Expression (fold change)
1.25
1.00
0.75
0.50
0.25
0.00
EGFP shRNA
stwl shRNA
wee shRNA
EGFP shRNA
stwl
wee
D
FLAG fusion: Pyd Stwl Klp10A CG13605
HA-Wee: – + – + – + – +
HA IP
anti-Flag
HA IP
anti-HA
totals
anti-HA

Supplemental Figure Legends

Figure S1, Related to Figure 1

Transcript versus protein expression for protein kinases and phosphatases. Comparing RNA-Seq data derived from a *D. melanogaster* developmental time course (Graveley et al., 2011), in Reads per kilobase of exon model per million mapped reads (RPKM) per transcript, to median signal-to-noise ratios derived from MS1 feature intensities across all matching peptides observed for each corresponding protein kinase (A) and protein phosphatase (B) during shotgun mass spectrometry. Represented is an average RPKM value from two time points comprising stages 1-8.

Figure S2, Related to Figures 2 and 3

Characterization of the transgenic protein kinase and phosphatase shRNA collection.

(A) Plotted is the cumulative number of lines in the collection capable of achieving a particular extent of knockdown in early embryos with a germline specific Gal4 driver. The number of transgenic lines capable of generating that specific degree of knockdown or better is indicated next to each data point. Lines that fail to generate eggs are not included.

(B) Based on qPCR analysis of embryos derived from the germline of females expressing a distinct shRNA, at least one of two shRNAs targeting the same protein kinase or phosphatase will generate 60% knockdown or better for the corresponding gene at a frequency of 86% (N=81).

(C) Considering those shRNAs that unambiguously target the coding sequence (CDS), or the 5’ or 3’ untranslated region (UTR) of all transcript isoforms, we find shRNA design influences knockdown. 81% of lines expressing an shRNA targeting the CDS generated greater than 60% knockdown, while only 14% of lines expressing an shRNA targeting the 3’UTR generated greater than 60% knockdown – annotated as ‘success’. The numbers of lines considered are indicated in parentheses. Plotted (y-axis) is the average transcript level (based on two independent qPCR measurements) remaining in 0-4 hour old embryos derived from females subjected to specific shRNA expression, relative to an shRNA targeting EGFP, versus (x-axis): (D) the average transcript level (units in RPKM) derived from

two time points encompassing the same developmental time (Graveley et al., 2011); (E) the concentration of purified RNA used for the corresponding qPCR measurement; and (F) the batch date of processing. Three reference genes were used for normalization.

Figure S3, Related to Figure 4

Reproducibility among replicate experiments. Plotted is the overlap in TMT reporter ion signal-to-noise (Sn) and phosphopeptide identity for six independent biological replicates of embryos (MTD-Gal4>UAS-*white* shRNA) labeled with three TMT labels (126, 127, or 128) and shot in two independent 6-plex experiments: (A) and (B).

Figure S4, Related to Figure 4

Phosphosite distribution in kinase deficient embryos. The distribution of abundance changes in kinase shRNA embryos relative to *white* control shRNA embryos for (A) unique phosphosites residing in seven shRNA-targeted kinases (*wee*, *gish*, *lkb1*, *grp*, *Tao*, *Slik*, and *Atg1*) plotted based on downregulated fold change where 1-fold indicates no change and (B) all unique phosphopeptides plotted as a log2 ratio. The distribution in all cases centers around zero.

Figure S5, Related to Figure 5

Enrichment for kinase-substrate pairs among phosphosite correlations, and the characterization of *slik* deficient embryos and *Drosophila* S2 cells treated with *slik* dsRNA or insulin.

(A) Correlations in changes in levels (>1.5 fold relative to a control shRNA) between any two phosphosites (PS) were identified from kinase-deficient phosphorylation data. 517 gold standard (YGS) kinase substrate (KS) pairs in yeast (Sharifpoor et al., 2011) were mapped to *D. melanogaster* proteins with DIOPT (Hu et al., 2013). 179 human kinase phosphorylation motifs from the NetPhorest atlas (Miller et al., 2008) were also used to predict *D. melanogaster* KS pairs. The distribution of

overlap between KS pairs and correlation pairs for 1000 simulated random correlation pairs of the same size is shown in grey (expected). The observed number of KS pairs among all correlation pairs is indicated (red arrow). Illustrated is the number of pairs when requiring PS correlation among at least two (top) or three (bottom) kinase-deficient profiles. Z-Scores and P-values are indicated.

(B) Lysates from 0-4 hour embryos derived from females expressing an shRNA targeting *slik*, *wee* and an *EGFP* control shRNA were analyzed by immunoblotting with a Stat92E antibody. Immunoblotting with anti-tubulin serves as a loading control.

(C) Plotted (y-axis) is the level of *slik* transcript remaining in *Drosophila* S2 cells treated with dsRNA targeting *slik* relative to a dsRNA targeting *EGFP* (left) and in 0-4 hour old embryos derived from the germline of females subjected to specific shRNA expression relative to an shRNA targeting *EGFP* (right). Three reference genes were used for normalization.

(D) Lysates from 0-4 hour embryos derived from females expressing an shRNA targeting *slik* and an *EGFP* control shRNA were analyzed by immunoblotting with a phospho-ERK antibody (dpERK). Immunoblotting for total ERK and tubulin serve as loading controls.

Sixty-nine phosphoproteins downregulated >1.3 fold in *slik* deficient embryos and upregulated >1.3 fold in *Drosophila* S2 cells under conditions of insulin stimulation are plotted (E) in log2 scale according to maximal change in *slik* deficient embryos relative to control shRNA embryos, and (F) in log2 scale according to maximal change in insulin treated cells relative to untreated cells.

Figure S6, Related to Figures 6 and 7

Characterization of *wee* deficient embryos.

(A) Lysates from 0-4 hour embryos derived from females expressing an shRNA targeting *wee* and a *white* control shRNA were analyzed by immunoblotting with anti-Cdk1-pTyr15, anti-HH3-pSer10 and anti-HH3-pSer28 antibodies. Immunoblotting with anti-tubulin and anti-HH3 serve as loading controls.

(B) Approximately 6400 phosphosites identified in *wee* deficient embryonic lysates were ranked according to degree of change relative to control. Indicated are motifs encompassing phosphosites

that are enriched among those phosphosites downregulated >1.5 fold. Motif-X was used to identify motifs (Chou and Schwartz, 2011). The PLogo tool was used to generate motif logos. Favored amino acids at corresponding positions are indicated above the line while disfavored amino acids are below.

(C) Plotted (y-axis) is the transcript level of *stwl* and *wee* remaining in 0-4hr old embryos derived from the germline of females subjected to specific shRNA expression, relative to an shRNA targeting EGFP. Three reference genes were used for normalization.

(D) Lysates from *Drosophila* cells expressing HA-tagged Wee together with 3xFLAG-tagged candidate Wee substrates were subjected to immunoprecipitation with anti-HA antibody and analyzed by immunoblotting with the indicated antibodies.

Supplemental Tables

Table S1: *D. melanogaster* protein kinase and phosphatase expression and orthologs, Related to Figure 1

Table S2: Transgenic shRNA knockdown and phenotype data, Related to Figure 2A

Table S3: Correlation between germline clone, mutant and shRNA phenotypes targeting the same gene, Related to Figure 3

Table S4: Control shRNA replicate phosphoproteomic experiment data, Related to Figure S3

Table S5: Protein kinase shRNA phosphoproteomic experiment data, Related to Figure 4

Table S6: All correlative phosphosite pairs in phosphoproteomic data and predicted *D. melanogaster* KS pairs from NetPhorest, Related to Figure 5A

Table S7: Insulin-stimulated phosphoproteome time course data from S2 cells, Related to Figure 5C

Extended Experimental Procedures

Transgenic shRNA line generation

Transgenic shRNA line generation was essentially as described (Ni et al., 2011). Twenty-one base pair shRNAs were cloned into either VALIUM20 or VALIUM22 and injected for targeted phiC31-

mediated integration (Groth et al., 2004; Thomason et al., 2001) at genomic attP landing sites: P{CaryP}attP2 (3L: 68A4) or P{CaryP}attP40 (2L: 25C6). The genetic background was y[1] sc[1] v[1]; P{y[+t7.7]=CaryP}attP). Selection was based on vermillion eye color. All lines were sequenced to confirm identity of the shRNA and miR-1 scaffold. More than half of the shRNA collection can generate knockdown both in the soma and germline (VALIUM20), permitting interrogation of protein kinase and phosphatase function spatially and temporally via different drivers. The others were constructed in VALIUM22, which is optimized for germline specific expression (Ni et al., 2011).

Quantitative real time PCR primer design

D. melanogaster primer design for quantitative real time PCR was as per (Hu et al., 2013).

Gene	FWD Primer Seq	REV Primer Seq	efficiency	r-squared
aay	AGATCGTCTGTTTCGATGTGGA	ATCGCCTCCTTGGTAACGC	102	0.996
Abl	GGGTCTCAACATATTCACCG	GTGAGGTAATGGACGCGACTG	105	0.999
Acf1	CAAGAACGAAACATTCCACGAC	GTGCCGGAAGTAGTGTTCATAG	102.1	0.997
Ack	CCAGCAGAGCGACCCACTTT	TTGGACTCGTGGTGACTTCG	97	0.997
Akt1	GTTTGGGAGGTGGAAAGGAT	CCCGTAAACTCCTTGTCGAA	103.6	
alc	CGACCATCAGTACAAGTTCTGCG	TTCTCTGTCCCTCGGCGTTC	94.7	0.999
ald	GAGAACGAAAACAGCAGCCG	GACACTCGGCGAGGTAGCATA	106.4	0.999
alph	ATGGGCGGATTCCTGGATAAG	GAGCGTAGTAGGCGTCCTC	103.8	0.998
Argk	ATGCCGAGGCTTACACAGTG	CATCGCCAAAGTTGGAGGC	98.6	0.996
Asator	TTGAAGCAATTTCTGGAGCACA	CATACACCTCTCGAACAAACCG	97	1
Atg1	CGTCAGCCTGGTCATGGAGTA	TAACGGTATCCTCGCTGAGCG	112.4	0.996
aur	AGTATGCGCCACAAGGAACG	CCTGAATATAGGTGGCCGACTGG	99.2	0.998
babo	GCGAAAAAGCCAGAAAACA	CATATATTGTTCGATTCCTTGCAC	109.6	0.994
bsk	TACGGCCCATAGGATCAGGTG	TGCTGGGTGATAGTATCGTAAGCG	98.5	0.998
Btk29A	GGGCATACGGTGTGCTGATG	CACACGCTCCACAACCTCG	104	0.999
Bub1	CAAATAATCCATCAGCCTCCG	GGGAATCGGAGAAGCAGGTG	116	
caki/CASK	TATGTCGTGTTTATAGCGGCG	CTCCAGGCTGCCGTCGTAAT	123.5	0.993
CamKI	AGCAGAAACATTCACGGAACCG	CTGTAGCGGCGTAGTAGGCTTG	101.4	1
CamKII	AAAGGAGCCCTATGGGAAATCG	CCCAAAAGGGTGGATAACCG	101.7	0.999
CanA-14F	TGATCACCATCTTCTCGGCG	GCCGGATGTTCATCACGTTG	97.6	0.997
CanB2	CGCTTCGCCTTTCGCATCTA	CGCGAATCCGATCGTCTTGT	99.7	0.997
cdc14	CATCAAGCCAAAGAACACGGT	GCGGACCAAAGTCATTGTAGAA	98.9	0.998
cdc2c	CATGCCACAACCCATAACCG	GCAGGTTGGGATCATAGCACAG	103.7	
cdc2rk	TATCCAATCTGCTGATGACCG	GCTAAACATGCGGGCCAGTC	95.7	0.996
cdi	ACTGCTGTCTGTACGATGCC	CTCGTGCTCGTATTTCTCCA	96.6	0.999
Cdk12	CTGCACTGGGAAGCAACCTG	GGAGGAGGAGAACGAAGCcG	120.5	0.997
Cdk4	ATGTGGAGCAGGATCTTTCG	CCGGTCAGTAGTTCCCTTGACA	103.7	0.999
Cdk5	AAGAAACTCACCCTGGTCTTCG	AGACGGCCATGTCGATCTCC	91.6	
Cdk8	TCAATGTGATGGGCTTTCCG	AGCGTATGATGTTCCGGCATC	100.8	0.997
Cdk9	GACAAATTGCTGACCCTTGATCC	GTGATTCAGAGCTGTGTCCG	91.4	1

CG10089	ACATCATCGCCATACATGACAG	AGACGGAAAAGTATTGGGAGAGA		
CG10376	TTCAAGCGATTTCTGGTCAGC	CCGGACACTTTGTATGTCTCATT	105.3	0.998
CG10417	GGTGCCTATTTGTCCCATCCG	CGCCATCCTTGCATAGAGC	105.5	0.997
CG10702	CAACGACCAGGAGGTGCAGT	CCAGCTTAGCTTCACAGACCG	100.2	0.998
CG10738	ATGTTTGCTCACCCCTGTCC	CCGGAAGTTGCTAAAAGCGAG	105.7	0.993
CG11486	TTGATATGCAGGAGGACGAG	CAGATTAAAGTCGGGTCGCT	99.9	0.998
CG11597	GCGACATCCGGCACAAGTTA	CGAAAGGCACTCCTCGTAGAAT	78.8	0.998
CG11870	GACCATTGGCGTCAGTGAACC	CACTGGTTGTATGGCATTTCCG	99.9	0.989
CG12091	CAACCTGCGACACAAGTACAA	GAACGATGAAAACTCTCCGGG	93	0.998
CG12237	GCCTTCGACTTCGACCACA	GGTATGCCACGAATGGTGTC	101	0.996
CG1227	GGGCTCCAGAGTTATTTACCG	GAGCACACAGCCAAGACTCCA	99.6	1
CG13197	GTGAAGGAGAATCTTCGGCTG	TGGCACTTGGGTGGTAGTATC	100	0.993
CG1344	CTGTAATGAGCTGTGTGCCG	CCCAGACAATATCGTCCTTATCA	106.6	
CG13850	AGCAAAAGCCAAGCCTCCAG	TCCGTGATAGTTAGCAGTCCAT	107.7	0.997
CG14212	GTTGAGCAGGACTCCTATTTGG	CGCACTTGGGGATCTGGTC	97.3	0.997
CG14216	TCAATGTGCGCTCCTACGG	GATGTCCTCGTATTTGGTGCC	104.6	0.996
CG14411	CGGACTGTTGAGTGTCACCAA	GGCCCAAATAGGTATTCTCCTGA	106.1	0.999
CG14903	ACTTGAATTCCGAGGACGCC	ACTGAGCTTGACCAGAGCAC	96.6	0.998
CG16771	CCGTGCAGCACACGAAATG	CACATGGCGGTTATCAGGAGG	85.6	0.997
CG17528	ATGCGATTATTGCTAAACAAGCG	GCGAACCACTTGCGTAATGG	106.8	0.995
CG17598	AACAGCGAGCGGGCTATTG	GGGGAACTTGTCCGGCATT	105	0.997
CG17698	TACGCGCAGGTCGATCTAATTC	TGATGGCAGGAGAGTATCCG	99.3	0.995
CG17746	GCGCCCTCGGTGACTATGTAT	CCAATCGTCCATGATTTTCCG	94	0.998
CG1951	CGGAGTGGGTCTGATGTGG	ACGACTTTTTCTCGAACACGAA	92.8	0.997
CG2124	CAAACTACCTCTGGCGAAGTG	AGGACGCAGTATTGCATACGG	104.6	0.999
CG3008	GTCCTTTCCGCCGGAGTTTC	CCTTATTGGAGAGCTTCATGTCG	104.8	0.998
CG31431	CCGATGATTTGTGATCTGTGGT	AAAACAGCGGGACTGCTGAAA	136.8	0.998
CG31643	TGCTCTTCTAACCCGACTGGA	CAGTGAGATTCCCATCACCAC	110.9	0.99
CG31751	CTCTACGGGATCACGATAAGCG	GGACAGTGGGTTACAATGAGG	104.7	0.998
CG32649	AAGAAGAAGTCCGACCAGCCG	GAGGGAACCTTGCGCTGTTT	100.7	0.999
CG32666	GACCTCAAGCCGCAGAACATC	CAGCTTCAATCCATCTTCTATGCG	97.6	1.000
CG34123	CTGGAGCCTGGATATTCACCG	GCATCGCCCACTTGCTTGGT	95.7	0.994
CG34380	TAACAGATGCTCAAATCACAGCG	GCATTCGACACCATGTGCTT	93.7	0.998
CG3530	GACAGGATCTCCGCTACTCAT	GCAGCGAAGTGTAGACATCGT	106.7	0.996
CG3608	CGATGCGACAACACAGTGA	ACCATGCATGCGAAAAGAC	101.2	0.996
CG3632	GGCGCACGGATGATGGTAT	ATCTCGCACCTGTACGGATTC	111.4	0.998
CG3837	CGGCTACTTCCAGACGCTAC	TGGCCACCAGTGAAGAAGA	102.4	0.995
CG4041	TGTTCTCGCATGTATTCCCG	ATCGCCCAGCATGAGTTTATCC	103.1	0.997
CG42327	GAAGTGCCACCTGGTTGTGAG	GTCTCAGGAAGCGGAATCACG	91.4	0.997
CG42637	GATGGAGAGCAACGGAGAGG	ATTGACCAGGCCACGTTTCT	97.4	0.998
CG43143	GGACAAGGCACTTACGGCAA	GATGGTTTTGATAGCCACCTCC	97.9	0.997
CG5026	GCTATGGTTGCTCCACAAGAA	AATCCCACCGACCACGATATT	97.3	0.999
CG5144	CCATGCCAGCAAAGGAAATGT	CAGCAGGGACTTGGATTTCG	105.5	0.994
CG5830	GACGACGAGCAACTGAACG	TGGCTTTAAACGATCCACATC	120.4	0.999
CG6498	CACGAATACTTTCTGGGCATGG	CACAAACTCTGCCTTCTGCCG	103.8	0.997
CG6697	TCAAAAGCTGCTCAACCTGA	CAAAGCGCTGATCTTCACAT	103.1	0.998

CG7028	CCACCGAACAAGCGAATCCA	GCTCAGCCCGCAATTTTGTG	103	0.998
CG7156	CGATTGTCTTCCCAAGGTCG	AGCCGCTTGACATCGTGGAAC	104.9	0.999
CG7207	GTATCCTGGCCCAGATTTCG	GAAGAACTCATCCTCGGGCAAT	100.8	0.998
CG7597/Cdk12	CTGCACTGGGAAGCAACCTG	GGAGGAGGAGAACGAAGCCG	120.5	0.997
CG7616	CTGAGCCTCGGAACACGGATT	AAATCGCAATACAGGACGACCG	108.1	0.996
CG8147	TCTCGGCCTGAGTGTTCTAGT	GATCCGGTTCCCATAAGCGA	95.1	0.999
CG8173	GACGAGCAGGGCGAGGTTAAT	CACTTCGTCTATGACCTCCG	106.7	0.996
CG8485	AGCATGAAAGTGGGAGATGCG	GGCTTCGGTTGGACTTGGTTT	94.7	0.999
CG8726	TGCAAGAGTACATAAACGCCG	GGTCGTGAAAGGACTGCGAGTA	94.9	0.999
CG8866	GCCAAGCACTTGGACGATGAG	GATGGTTCTCAATGAAGTGCG	107.9	0.999
CG8878	CCACACTACTGCACACCCCG	TGGTGACTCCATCACACTGGA	100.1	0.998
CG8964	GCGCCAGCATCATTTGAGG	CAGTTGGTAGTCACAGGGCAA	108.5	0.982
CkI-alpha	TATTGAAGGAAAGTCGCCCCG	GGTAAATGTCGCCAAACGATCC	96.4	0.999
Cks30A	GCCCAAGACTCATCTGATGACG	CCGGCTTATGGATCATGTAGTGG	100.7	0.997
Csk	GAGTTCGGTGACGTGATGCTG	CAGCCAGAAACTTCTGCACG	113.6	0.998
csw	GAACATGGTCTGGCAGGAGAAC	CTCCGATCTACCCTCGTCCG	102.4	0.998
Dd	TCGCCAAGTGCGAGCTTTTAT	CGTCCAGGTCCAGAACGAG	87.4	0.997
dnt	ATTGCCACAAGGAACTGCGTTAT	CCCCAGGCAGTTGTAGTCCG	108.3	0.997
Doa	AAGATTAACCGCGAGGTGCG	CCCGAAGTCGATTAGGCGAAC	97.6	0.998
drl	CCCAACTTGCTAACAATCGGA	CTCCCGCACGTAGTAAAGCTC	105.6	0.996
Dsor1	GGCGAGATCAGTATCTGCATGG	TGGACTCTGGTATTCGACCG	104.2	
Dyrk3	GGGCCATCGAGATATTATCCG	AGTTGGCCGAACTGTTTAACGA	104.5	0.995
EDTP	CTTTGAGGAAGGGACGGCGTA	AGTCGAGCTTAAACAGGTATTCG	95.5	0.999
Eip63E	CGAGGTGGTCACGTTATGGT	AGGTCGAGTACTCCGTGCTG	92.7	0.998
Eph	TTGGCACATGCAGATCAGGTT	TGGTGTTTGGGCTTGAGGTC	109.1	0.995
eya	CTACGACGGCAAACATGACTAC	CGCATAAGGAGTTCCGTATCC	89	0.997
Fak56D	GCTGACCGATGATTATGCCG	CGAACGGTGGGCGTAGAGTAG	110.9	
Fancd2	AAAGAAACCTCTGAACACCATCG	CCAGATGAGGACTCAACGGATA	95.6	0.997
Fcp1	AGCGACGAGGGTCCTGTAA	CTTCGCGCTTTCTCTTCAAC	106.2	0.999
fj	CAGCGGTCGTTATCGCAAG	GCTCACTGGTAGGATTTGTCGG	91.4	0.994
flw	CGTGGCCTCTGTCTCAAGTC	CAACAGGTCTGTGTACTGGC	103.4	0.997
for	CAGCGATTTCCTCAAGAGTGT	CTCCTCCAAAACATCGGAGA	101.6	0.999
Fps85D	ATATCGCTCTCCACAAATCGTC	CTGAGCACAATCTGGCTCTCC	103.6	0.999
fray	GGACACTGCCGAGGGTATCG	GTATCCAGCGCATCAACGAGTC	97.4	1
fu	CAAGGACGACAGCAAGGTGGT	AGCTCTTTCGTGGCTCTTCCG	104.8	0.999
GckIII	TGCATTATCGTCCTCTGTGTCC	CCTTCGTTGGCTGTAATGACCG	103.9	0.998
Gcn2	CCCTGGTGGAGAGTTTGATGC	GTTACACTTGTCTACAAAGTCGCG	100.4	0.998
gek	TCACCAAAGCGGATTTACCG	CCGGATGAACCAAAGACATTGC	100.7	0.999
gish	CCAAATTTTCGTGTCGGTAAA	GTTCATTGTTGTAAAGGTTTTTGC	104.7	0.999
Gprk1	TGGAAATGTTACTTCAAAGGGACG	TACTTCATCCGCGCCATTTC	99.7	0.999
Gprk2	AGCGAGAGAAGGTGGTTCCG	CATTGCGATATGTGTGGGAATTG	103.2	0.999
grp	TTCCTATGACCTGGTGGACTCG	AGACTGCAGACGCTGCCTCTTA	93.7	0.999
Haspin	GGCAACAGGAGATTATCAATACGA	CCAGTTGTTCTTTAACTCATTCCG	93.9	0.999
hep	CCCCGCCGACAACTAGAGTG	CACCACCGGGACCACTAGAAA	106.5	0.994
hipk	CAACAATGTCAAGGCATCCG	CAGGCTGCACAGTGTGGAAA	106	0.999
hop	CACCACCAACACCAATTCCG	GGAACGTCGTTTGGCCTTCT	115.6	0.996

hpo	CGAGCCATCTTTATGATTCCG	GGCACTTGCTCACGAAGTCAAT	93.1	0.997
hppy	ACAAGATCCCGGAGCGACTG	TGTGCAGCACTTTGTGTCCG	95.2	0.997
htl	GCTGCAGTCAAAATGGTCCG	GATTTCCGTGTGGCGCATAC	97.5	0.997
ik2	ATCTCGCAGATGCACAAACATT	TGGAGGAGGTCCATTGATCG	103.9	1
Ilk	GTCTGCGGGTCAAGATTC	TCCTCGTTCATGCAGATTGAAA	81.6	0.995
irbp	AGTTCATCACGTTGTCAAGAGC	TACGATCGGACAGGATTTCG	102	0.999
ird1	AGCACTGGAGGCACGATCAC	GTCCCATCTCCTCGTACTGCG	103.9	0.999
ird5	AAGTTTGCGAGAAAGACCTATTCG	GAAATTATCGCACCATTGCAGA	103.6	1
ire-1	ATGGTAAGGAGGGCGAGCAG	ATGACCGTGTACTGAGTCCG	106	0.998
JIL-1	ACGGTGGTCCAGAAGCGAAA	CCTCCAGTACCACTCTCTCCG	100.4	0.998
key	TTATCTTGGGTAGCTCGCCG	ATACGTCGGACCGCAAGGAACT	103	0.999
KP78a	TCAGACGCCACCCTTATCCG	GTGCGGTCAGCTTGGAGAAGA	103.4	0.998
KP78b	GTGGCAAGTATCGTGTTCCG	GTTGCGTTGGATTCAGAACGAG	102.5	0.999
ksr	ACAGCCGGTGTGGATAAGAGG	CATTTGACTTGTGGGTATCCG	103	0.999
l(1)g0148	CAACCAAACAGGCACGCAAC	ATCGAACAGCTTGCCAATGTC	100.8	0.999
l(1)G0232	CTATGGCGTTCCCAGCTC	CCTGCTTCTCACGCACCT	93	0.999
Lar	TCTGAATCTATCCTGCATTGCCG	GATCTTCGGAGCCCTTCATCC	92.7	0.999
lic	CAAACGCATACCCATGACCG	GGGCAGTCGCTGGATCTCAT	121.3	0.999
LIMK1	GTGAACGGCACACCAGTTAGT	ACTTGCACCGGATCATGCTC	106.3	0.999
Liprin-beta	GAGGGCAGCAAAATGCTCG	TAAGTTGCGTTCGCTGAGTGT	97.9	0.996
Lk6	CAAACGCCCAGTAACATCCG	GCTGTAGGACCACACGCTTGAC	102	0.999
lkb1	CCTGCTGCTCTCCCTGGATC	GTCGTGCATGTGTCGTCAGG	90.8	
loki	AATTTCAGTGATCCCGACCG	ACCACGCACGGATGTGAAAG	99.5	0.999
Lrrk	CCGCTTGTTCCGTTGTTGTG	ATCTTTCCTGCAATTTCGCCG	102.8	0.998
Madm	GCACTGCCGTGATGTATGTACC	GTGCCCGAGTGTTCTACGTCG	97.9	0.999
Mapk-Ak2	AAGTGCAGGAGGAGATGACG	GACTTGTCCAGCGCCTTGATT	103.4	1
Mat1	TGTCCAGAGTGCATGGTCC	GCCTACGAATATCCACCTCCTTC	93.4	0.998
Mbs	TACAAGGCGCTCTGGGAAGC	CGAGTGTTGCACGTGTCTGG	97.3	0.999
mbt	AAATCCACAGGTCGCCAGGT	TCGTTGAATAGCAGCTCCCG	98.5	0.997
mei-41	CCCTCTCTGGGAAGAATCGTG	CTTAACGCTCTCGTTGTCCG	99.5	0.998
Mekk1	ACAGCTTCCGCAGACTTACCG	CAGTCCATAGTGTTGCGCCG	102.5	0.996
Mipp1	ATGCGCCTGCTGATATTGCTA	GCGGTCTTCGAGGAGAACTG	96.8	0.996
Mkk4	GTTGCCGTGTATGTGGCTGATA	CCGTAAACTGCGTAATGCCG	95.9	0.998
Mkp	CAAAGGCGAATGGGCAACC	TCGCTCAATGTAGCGTACACC	102.3	0.982
Mkp3	CGACTCGGAAGCGTTGAAAAA	GTGATCCGTGATCGGAATCTG	88.9	0.999
MKP-4	CTCATCCACTGTGATCGCTTAC	GAAGAGCTTTAGTTGGCTGACA	96.8	0.993
mnb	GCACCATCACTCTAGTCCCTCGT	CGAAAGTGGTTGGGAATC	111.1	0.992
mop	CTTTGCGGCTTTGAAAAAGT	GGCATGGACCTCTTTGGAG	98.5	0.999
mos	TACCCTTACCGAAGCCTCCG	CGCTTGCAGTTGCCACATTGTA	102	0.999
Mpk2	GATGTTGGAGCTAGATGCCG	GCTGGGCTCCGCATACTTCT	104.2	0.998
mRNA-cap	CGGACAAAAAGAATCCCAAC	CTCCTTGGTGACTGGATGC	107.1	0.998
msn	TCCCTTGGACAGCAGCGATT	AGTTCCATCGTTCCTAGCCCG	98.8	0.997
mtm	GGCGGAGAAAACGGCATTC	CGGTAGTTGGTTATGGTAAGAGC	107.7	0.998
mts	GCAATCAGTTGACAGAGACACA	CACCGGGCATTTTACCTCCT	105.5	1
Myt1	AAACCAAGGCAAATCCCGTCT	AACACGGACTCTCGAAATCG	82.6	0.999
Nak	CCGCTGTGTCTCCTTACCCG	AGTCCGGGTGGCAAACTGAA	103.8	0.997

Nek2	GGCAGATGCAGGAAAAACTT	TCGGCTGTCTGCAACTACAA	106.7	0.997
Nipped-A	AGTCCGGCATATCCGTCGT	GAATGAACTGAGGTTCGCCAT	91.4	0.999
nmo	CTCCCTACTATCAACCGCCG	GCTCCATAGCCGATAGGACGA	92.2	0.999
otk	CGTATGACAAGCGTGTCCATC	ATAGTTGCCAACATCCTCCGT	91.3	0.998
p38b	GAAGCGCACCTATCGGGAAC	GACATCCAGCAGACCAATAACG	108	0.999
Pak	AGATGTACCGCCCGACATGC	TCTTCAGCGTTTTCTTCTTCCG	97.8	
Pak3	AAGACCAATCTGGAGCACCG	GGTACTGGTGGAGGCTCTTGC	102.4	0.999
Pdk	GCCATTAGCGGGCTATGGAT	CCATGGAAATAGCGGGCGTA	84.5	0.998
Pdp	GAGTTCGTTTACAACTTTCCCGT	CAGGGCCAGTTTGATCCCAG	107	0.998
PEK	TACTAGGTCCAGTGGTGCCG	GCTTGTCCAGGTGGGAAGCTA	112.5	0.999
Pez	TGTTTGTTATATCAGTGCATCACCT	AGCTGATCGTGCAGTCCA	93.9	0.999
Pgam5	GTGAAGGAGCGCCTATTCCG	GGTGGAAGTATCGGCGAAAGC	92.4	0.998
PhK-gamma	GGAGTGGGCTGATATTTCAGAGG	GGATCAACGACTAGACATTTGCG	105	1
phl	GAAGGCGACAGCGATCTATAC	CAGGTTGGCAAACTTGGCA	101.9	0.987
Pink1	CATAGCCAAAGGTTGTGCCG	ATCCGAGGCAACATCTTTCTTGA	95.3	0.998
Pk17E	GTGATGGCGCTCCAAAGGAT	TCCCTGGCTATAATCTCCCG	88.8	0.998
Pk61C	TGCTTAGTGCAGAATTAGGCG	GGCATCGTTCAGGTCGAAAG	104.7	0.999
Pk92B	GCCGCTGAGCTACAACACAA	GAATGCGTTATGTCCAATTCCG	102.8	0.998
Pka-C1	GCACTACTTGGACCTCATCTACCG	CACCTTGAGGTAGCCCTGCG	112.6	0.998
Pka-C3	GGCGTACAAAATTCCATCAAACA	CTCGCTGTAATCGGACTCCA	106.5	0.997
Pka-R2	CAGGAAGCGGAAAATGTACG	GCCAGATTCATGCGTTCGTAGT	97.9	0.998
Pkc98E	CAAGGAGCAGGAGTACGGCG	GGCCAGCCATCATCTCGTACA	122.2	0.998
Pkn	GCCATAGCCGTGATGCGTAG	ATGCCTGTTTCTTAACATCCTCCG	100.2	
Plip	CGTTTCCTTCTACCCCACCC	CCCAGTATCACATGCTCATCG	103.8	0.995
pll	TGCAGCAGAGCTACAACGAA	CAGGATATTGTCGTGCCGGA	98	0.997
png	GGGTCTTCCTCTGCCACCAA	CAACTCTGTCTTCGGATTCCG	92.4	0.995
Pp1alpha-96A	TGCACGACCGGGAAAGAATG	AGCTCCAGGAGTATGGGCTG	106.6	0.998
Pp2A-29B	CCACCATTGCACTCGCTTTG	GGAATCAACTCGGACCGTGT	109.4	0.999
Pp2A-B - 19738	TCCTGAAGACTGTTTTACATCGC	CTATGCCATTATGATGCTCCGTT	106.3	0.996
Pp2B-14D	CAATAGTACCGCCTCGAACAAC	GTGCAGCTTTCCAGTGCTC	105.8	0.989
Pp2C1	GATGAGTCGTCCGTGGAATTT	GCTGATCCTCTCTGGCCTTTG	95.2	0.997
Pp4-19C	CAGTTGGTAATGGAGGGCTT	CGCAGCGATAGCAGTAATTG	94.5	0.998
PpD3	ATGCTCAAAACCAAGGAGTTCTC	ACCATCCTGTAGTGCGAAACC	82.2	0.999
PpV	ACCGTTTGCGGTGACATC	AGTTGGTATGCGGCACCT	112.1	0.999
PR2	GACGCGCCATCGAAGTAGTG	GTTCTCGTATTCCCGCTCCG	97.8	
primo-1	GTGCTAATGATTTGTTTGGGCAA	TGCTGCACTATCGACCTCCA	94.1	0.999
PRL-1	GAGACACAAGGCATTACCGTC	CTTTAAGACCTCAAACCACTCGT	101.8	0.997
Pten	ACATCATCGATTTCTGATTTGC	CAGTTTCCGGCGATGTAAAA	94.2	
Ptp10D	GCTGTACTACACGAACTTTACGC	CTGAACGGACAGATTCGACGG	93.2	0.999
Ptp4E	ACCACGACTGGAGCATATCA	GCCATGTGGTGAAGTGAAAG	93.2	0.999
Ptp61F	AACGGCATCGATCCAATTC	CCGCTTCAGCTCGTTCTC	104.8	0.997
Ptp69D	GTGCGATATGTGTGCAAGGAT	GCTACTGCTTCGTTTTCAGATGC	107.5	0.998
Ptp99A	GGGAAGTGCCCGTTAAGATCG	CTGAATCCAATGTCCCCGTC	101.2	0.996
PTP-ER	TGCCCTACATTAATGCCAATTAC	GTAGCGCTGCGTGTTCTG	90.6	0.995
Ptpmeg	GTCGTGAGATGGGTTGATGCT	CGGCTGGGATCGCTTACAAAA	105.8	0.997
puc	TCCGGCGGTCTACGATATAGAAA	AGCAATAGATGCGGGAAAACG	90.8	0.998

put	TTTTGCCCGGAAGTCATGGG	TGCTCTATCCGTGTTTCACATTG	109.9	0.985
PVR	CAACCCTCGGACACTGGTCTA	GTAGGTGGCACGTTGTACGTT	110.6	0.996
rok	TACGAATGCAAGAGATGCCG	CGGGTCGTGTTTGTCCACAT	100.7	0.999
rolled	ATGGCATGGTTGTGTCTGCG	AAGTTTGGTGTTCAAAGGGCGATA	97	0.999
S6K	TCCTTGGCAAAGGTGGTTAT	ATTGGTCACAATGGATGCC	92.6	0.998
S6kII	CTTATGGAGCTGAGTGATTCCG	CCCTTCTCTCCTACCGCCAGTT	94.9	
SAK	TGCACACTCACCAGGATGTG	ACGCGGTTAGTGAGTCCAGTGC	99.5	1
sax	GAATGTGGTCTGCTGTGCCG	TGTCGAAGGGCAGCAGTTCC	102.9	
Sbf	CGAGGGCATTGAATGGTT	GATGTCCGTCAGCACAGAGA	101.3	0.996
sgg	AATGTATCGTATATCTGCTCCCG	CAACCGGCACTCCAGACATC	99.1	0.999
shark	CAAGCTGACGGTGCCCTTGAT	GCAGCAGATTGGTCACTCCG	102.9	0.997
Sik3/CG42856	AGATGCAATGCTGCCAGGAGAA	GCATATAGCTTTGCAGCTCCTCG	102.5	0.999
slik	GGGAGGCACTTCTCTGGGAAC	GCATAGTTCCTTTACATGCCG	97	0.998
slpr	GCACCTATTCCAAATTCTCCG	CCCGTTATCAGTTCCCACAGC	94.8	0.998
smg1	AGGCTTACCAATGCAAAGGCG	GATGATCTTGGACAGACGCAGA	96.9	0.999
smi35A	TCAAATGCAATACGCCCATGA	TCAAGATCGGTTAGGTAGTTGCG	108.5	0.999
SNF1A	TGGGCACTACCTACTGGGCG	ATCTGGTGCTCGCCGATCTT	101.6	0.998
SNF4A-gamma	CCGTAGAAGTGTCCTTTGCCG	AACGCTGGCTGGTCATCATC	117	
spag	GTCATGTCCAGACAGACAAGTC	CTGGCAAGTCCTGTTTCTCCG	99.4	0.998
Src42A	GGAGATACTGAATGACACGCAG	GGATGGAATGTAGCCTTCCGAA	110	0.997
Src64B	AAGAAGTTCCGACACAACCG	ACGATGTAAATGGGCTCCTCCT	104.2	1
SRPK	ATCCGCTGACTGAGGGCACTG	GTAGAGTTTTCCAGTTGTGGCG	102.3	0.998
Stam	ATGCCGCACAGATGAACTCG	GGGAGTCGGCTGAGTGTAGATTG	98.6	0.998
stg	GAAAACAACTGCAGCATGGAT	CGACAGCTCCTCCTGGTC	97	0.998
Stlk	AACTGTTCGTCGGCTTCAACAT	GCTATTGCAACTTCCGGAAACC	92.7	
Tak1	GCCAACTGGACAATAATCCG	TGCTCTCCTCCTCGGGAATC	97.9	
Tao	AGACACAGGAGCTGGAGTACCG	TCGTGTTGCTTGTTTATCTGCTC	101.6	0.999
tefu	GGGATTCGATAAACTGGCCG	AAAGGCAGCAGGCAGGTCTT	152.8	0.993
tkv	ATGGAACCTGCGAGACCAGAC	CTCCTCGTACATCCCGGTCG	104.1	0.998
torso	CATGATCTGCCGCACGGAGT	GTAGGTGGCATTTGGAGCCG	105.4	
trbl	CCACTTGGTCGATCTAACCG	TCGTTTACAATACGGCAGAGGAA	93.1	0.994
trc	GCCCAGAAGGAGACGGAGTATC	CCTCAAAGTCCTCCACACCG	110.5	0.996
twe	ACGTATATCGCAAATAGATCAGGA	CACACGCTCCACTTTCATCA	116.9	0.999
twf	CCCTTGGCGTGGAGGTTGTTA	AAGAAGGCTTCGGTCAGCTCG	88.9	1
tws	GGAAACAAAGCCCATTGAGA	CGAAGATGCAGTCATTCTCGT	100.2	0.999
wdb	GGCACGTTTGTGGATCGAATC	GCAGCTCAACATCCTGAGAAT	101.9	0.997
wee	ACTCGATGCGCGAAATCCAC	TTGACTTGCATGAACTCCCG	119	0.993
wnd	CATTCAGCAACAATCAACAACG	CATACACTTCACAGGGGACTCCG	101	1
Wnk	AGCCGAACCCGACATCAAAA	GTGTGCAGAAAGTGTGCCCT	97.2	0.999
Wsck	TTCGGAATGACAATGGACCG	GGCGTTGTCCACGTATTCCAC	104.7	0.997
wts	AGGACGGTGGGTAATCCAGGT	GAGCCACCTCACTGAAACCG	91.4	
yata	GCCTCCGATTATGGCAACAAC	ATCCTGAGAGGTATCCATTTCG	98.6	0.998

Embryonic RNA isolation

Approximately 300 embryos (0-4 hours old) were collected and incubated in 50% bleach for 5 minutes to remove chorions. Post washing with 0.1% TritonX-100, 50 microliters of TRIzol (Life Technologies) and an equal volume of RNase-free 0.5 mm glass beads (Next Advance) were added to de-chorionated embryos in an Eppendorf Safe-Lock 1.5ml microcentrifuge tube. Homogenization of embryos was by bead beating at 4^0C at a setting of 8 in a Bullet Blender (Next Advance), 3 consecutive times for 3 minutes. Lysates were stored at -80^0C until further processing. RNA was extracted with chloroform and precipitated with isopropanol. RNA pellets were resuspended in RDD buffer (Qiagen) and incubated at room temperature with DNAse I (Qiagen) for 10 minutes. Samples, diluted in RLT buffer and ethanol, were further processed for cleanup with an RNeasy MinElute Cleanup Kit (Qiagen). RNA was eluted with RNAse-free water and RNA concentration and purity (criteria: A_{260}/A_{280} ratio near 2) assessed using a Nanodrop 8000 spectrophotometer (Thermo-Scientific). All samples were processed alongside an EGFP shRNA-expressing sample as a control.

Embryonic cDNA generation

A total of 1 microgram of RNA was incubated with iScript reaction mix (a mix of oligo(dT) and random hexamer primers) and iScript reverse transcriptase (iScript cDNA Synthesis Kit, Bio-Rad) for reverse transcription. Reaction conditions were: 5 minutes at 25^0C, then 30 minutes at 42^0C, then 5 minutes at 85^0C.

Primer evaluation by thermal analysis/calibration curve analysis of PCR products

cDNA isolated from embryos expressing a control shRNA targeting EGFP was diluted serially four times by a factor of four, starting with $1/20^{th}$ of the cDNA synthesis reaction volume. A no-template control was included to assess the likelihood or primer-dimers. Each primer was added to a final concentration of 0.4 micromolar in iQ SYBR Green Supermix (Bio-rad) with a final reaction volume of 13 microliters. Bio-Rad CFX Manager was used to calculate R-squared values and PCR efficiency for primer pairs (Table S2), based on the results of a two-step program (40 cycles, alternating between 10 seconds at 95^0C and 30 seconds at 56^0C) with a Bio-Rad CFX96 Touch Real-Time PCR Detection System. Melt curve analysis comprised temperature ramping over 5 minutes, from 55^0C to 95^0C in 0.5^0C increments. Criteria for primer validation are described in (Hu et al., 2013).

Transcript knockdown assessment in shRNA-expressing embryos

Germline-specific expression of shRNAs targeting EGFP (control) or various protein kinases and phosphatases was induced using the Gal4-UAS system (Brand and Perrimon, 1993). Specifically, 70 females heterozygous for the UAS-shRNA and either MTD-Gal4 (Petrella et al., 2007), a line

expressing three Gal4 drivers sequentially throughout oogenesis, or tub-Gal4, a line expressing Gal4 from a maternal tubulin promoter at two insertion sites during mid and late oogenesis (Staller et al., 2013), were crossed to 40 UAS-shRNA males to recover fertilized embryos. RNA was isolated as described above, from approximately 250 embryos (0-4 hour old) derived from Gal4/shRNA females cultured at 27^0C. cDNA was synthesized from 1 microgram of purified RNA as indicated above. cDNA synthesis and quantitative real time PCR analysis was carried out twice, with technical triplicates, using validated primers in iQ SYBR Green Supermix (Bio-Rad), with a CFX96 Real-Time PCR detection system (Bio-Rad). Query gene expression was relative to a control sample, normalized to the expression of three reference genes: *ribosomal protein L32*, *alpha-tubulin*, and either *nuclear fallout* or *Gapdh1*, using the $\Delta\Delta$C(t) analysis method. These reference genes range in expression from high to low in 0-4 hour embryos, based on RNA-Seq data (Graveley et al., 2011). The extent of knockdown is reported as 1) an average of the remaining transcript relative to two independent reference genes; and 2) a single remaining transcript value derived from comparison to the reference gene for which the control sample and the knockdown sample are closest in terms of cycle threshold (Ct) value for that specific reference gene (the preferred method).

Stat92E target gene expression in *slik* shRNA and *EGFP* shRNA-expressing embryos

cDNA was synthesized from 1 microgram of RNA purified from *slik* shRNA and *EGFP* shRNA-expressing embryos as described above. Quantitative real time PCR analysis was carried out with technical triplicates using validated primers (Rajan and Perrimon, 2013) in iQ SYBR Green Supermix (Bio-Rad), with a CFX96 Real-Time PCR detection system (Bio-Rad). Query transcript detection was normalized to the expression of the reference gene *ribosomal protein L32*.

Immunoblotting of embryos

Embryos were collected and incubated in 50% bleach for 5 minutes. Post washing with 0.1% TritonX-100, an equal volume of 2x SDS loading buffer was added to the dechorionated embryos in an Eppendorf Safe-Lock 1.5ml microcentrifuge tube. Homogenization of embryos was by bead beating at 4^0C at a setting of 8 in a Bullet Blender (Next Advance) for 3 minutes. Samples were boiled for 3 minutes and spun at 13,000 rpm for 2 minutes. Twenty micrograms of protein was loaded per SDS-PAGE lane for immunoblot. Primary antibodies to assess knockdown included: anti-Fused (Hybridoma bank 22F10); anti-Wee (a kind gift from T.T. Su); anti-Grp (a kind gift from T.T. Su); anti-Punt (Abcam ab14680); anti-Cdk8 (Abcam ab52779); anti-ERK (Cell Signaling #9102); anti-NAK (Abcam ab109693); anti-CKS2 (Abcam ab155078); anti-AMPK alpha (Abcam 80039); anti-Ptp69D (Hybridoma bank 3F11); anti-Ptp10D (Hybridoma bank 8B22F5); anti-Csw (L. Perkins); anti-Mts (Cell Signaling #2259); and anti-Ptp99A (Hybridoma bank 3A6). Other antibodies in this study included

anti-Cdk1-pTyr15 (Cell Signaling #9111); anti-Akt-pSer473 (Cell Signaling #9271); anti-Stwl (a kind gift from D. McKearin); anti-pTyr (Cell Signaling #9416); anti-Stat92E (a kind gift from S. Hou); anti-dpERK (Cell Signaling #4377); anti-ERK (Cell Signaling #4695); anti-HH3-pSer10 (CST#9701); anti-HH3-pSer28 (Abcam ab5169); anti-tubulin (Sigma T5168); anti-HA (Roche 11867423001); and anti-FLAG (Sigma F3165).

Embryo preparation for mass spectrometric analysis

Eggs were collected, dechorionated with 50% bleach for 5 minutes, washed with 0.1% Triton X-100, sorted under the microscope to remove any contaminating aged embryos, and delivered to denaturing urea buffer for lysis. Embryos were lysed with a glass homogenizer on ice in: 8M urea, 75mM sodium chloride, 50mM Tris-HCl pH 8.2, 1mM sodium fluoride, 1mM β-glycerophosphate, 1mM sodium orthovanadate, 10mM sodium pyrophosphate, 1mM PMSF, EDTA-free Protease Inhibitor Cocktail Tablet (Roche). Lysates were stored at -80^{0}C until further processing. For quantitative phosphoproteomic analyses, one milligram of protein (approximately 700 embryos) from each sample was reduced with 5mM dithiothreitol at 56^{0}C for 25 minutes. Cysteines were alkylated with 14mM iodoacetamide for 30 minutes at room temperature in the dark. Unreacted iodoacetamide was quenched by incubation with additional dithiothreitol to 5mM for 15 minutes at room temperature in the dark. Lysates were diluted 1:5 with 25mM Tris-HCl, pH 8.2 and calcium chloride added to 1mM. Digestion with 5 micrograms sequencing grade trypsin (Promega) was overnight at 37^{0}C with agitation. Peptides were acidified with 10% trifluoroacetic acid and desalted using 1cc Sep-Pak tC18 solid-phase extraction cartridges (Waters). Eluted peptides were lyophilized, resuspended in 200mM Na-HEPES pH8.2, and labeled with TMT reagent (Thermo Scientific) in anhydrous acetonitrile (2 milligram TMT reagent per sample) for 1 hour at room temperature. TMT labeling was as follows:

Experiment 1: Cdk8 shRNA: TMT126; *Cks30A* shRNA: TMT127; *mei-41* shRNA: TMT128; *tefu* shRNA: TMT129; *wee* shRNA: TMT130; *white* control shRNA: TMT131

Experiment 2: Atg1 shRNA: TMT126; *cg3608* shRNA: TMT127; *Csk* shRNA: TMT128; *Gprk2* shRNA: TMT129; *Pak* shRNA: TMT130; *white* control shRNA: TMT131

Experiment 3: Bub1 shRNA: TMT126; *cdc2rk* shRNA: TMT127; *Eip63E* shRNA: TMT128; *grp* shRNA: TMT129; *slik* shRNA: TMT130; *white* control shRNA: TMT131

Experiment 4: gish shRNA: TMT126; *lkb1* shRNA: TMT128; *mos* shRNA: TMT129; *Tao-1* shRNA: TMT130; *white* control shRNA: TMT131

Reactions were quenched by the addition of hydroxylamine to 0.3% and incubation at room temperature for 15 minutes. Labeled peptides were combined, lyophilized, and stored at -80°C until

further processing. Samples were acidified with 10% trifluoroacetic acid and desalted using a 3cc Sep-Pak tC18 solid-phase extraction cartridge (Waters). Phosphopeptides were separated by strong cation exchange chromatography (SCX: (Villen and Gygi, 2008). Lyophilized peptides were resuspended in SCX buffer A (7mM potassium phosphate, pH 2.65, 30% acetonitrile) and injected onto a SCX column (Polysulfoethyl aspartamide, 9.4 mm×250mm, 5 uM particle size, 200 Å pore size, PolyLC). A gradient was developed over 35 min from 0% to 30% buffer B (7mM potassium phosphate, pH 2.65, 30% acetonitrile, 350mM potassium chloride) at a flow rate of 2.5 ml/min. Twelve fractions were collected and lyophilized. Peptides were then desalted with 1cc Waters Sep-Pak tC18 solid-phase extraction cartridges and subjected to titanium dioxide based phosphopeptide enrichment (Kettenbach and Gerber, 2011) using 500 micrograms titanium dioxide microspheres (GL Sciences) per milligram protein. Eluates were further desalted using STAGE tips (Rappsilber et al., 2003) and lyophilized. Samples were reconstituted in 5% formic acid / 5% acetonitrile.

For shotgun mass spectrometry, 1 milligram of protein was alkylated and digested peptides were subjected to SCX fractionation into twenty fractions without labeling and desalted eluates lyophilized and reconstituted in 5% formic acid / 5% acetonitrile.

Preparation of *Drosophila* cells for mass spectrometric analysis

Confluent *Drosophila* S2R+ cells grown in Schneider's Medium (Gibco) supplemented with Fetal Bovine Serum (FBS) (final concentration of 10%), Penicillin (50 units/milliliter final concentration), and Streptomycin (50 micrograms/milliliter final concentration), were serum starved for 1 hour. Fresh media with insulin at a final concentration of 5 microgram/milliliter was then added to the cells. After 10 and 30 minutes the media was aspirated and cells were lysed in denaturing urea buffer on ice. Lysates were stored at -80^{0}C until further processing. One milligram of protein from each sample was processed for phosphopeptide purification and mass spectrometry as described above for embryonic lysates. TMT labeling was as follows: untreated, biological replicate #1: TMT126; untreated, biological replicate #2: TMT127; 10 minutes insulin, biological replicate #1: TMT128; 10 minutes insulin, biological replicate #2: TMT129; 30 minutes insulin, biological replicate #1: TMT130; 30 minutes insulin, biological replicate #2: TMT131.

Mass spectrometric analysis

Ratio distortion in isobaric quantitative proteomic experiments is a major concern due to interference by contaminating ions in the isolation envelope subjected to MS/MS (Ting et al., 2011). We reasoned interference should be less of an issue with phospho-enriched samples: we anticipated 4

phosphopeptides to be isolated for each protein (4x 6,980 = 27,920 phosphopeptides) based on the average number of phosphosites per protein found to date in yeast (Amoutzias et al., 2012). The predicted number of peptides generated by digestion of the *D. melanogaster* proteome with trypsin is 321,297 (Brunner et al., 2007). We therefore estimated a phospho-enriched mixture would have approximately 10-fold reduced complexity compared to the entire proteome, thus justifying our rationale for proceeding with MS/MS-based analysis. Moreover, the 12% reduction in protein quantifications observed with an alternative MS^3 method (Ting et al., 2011) would translate to an even greater loss for phosphopeptide quantifications given that individual protein quantifications are an average of many peptide measurements while phosphopeptide quantifications are derived from a single measurement. For these reasons we decided to proceed with MS/MS based analyses.

Samples were subjected to LC-MS/MS with an Orbitrap Velos Pro mass spectrometer (Thermo Scientific) using higher energy collision dissociation (HCD: (Olsen et al., 2007) and a top ten method (Dephoure et al., 2008). MS/MS spectra were searched against a composite database of *D. melanogaster* proteins derived from Flybase version 5.23 in both the forward and reverse orientation using the Sequest algorithm (Eng, 1994). Search parameters included: a precursor mass tolerance of 20 ppm; up to two missed cleavages; static modification of TMT tags on lysine residues and peptide N termini (+229.162932 Da) and +57.021464 Da accounting for carbamidomethylation on Cys; dynamic modification of phosphorylation (+79.966330 Da) on Ser, Thr and Tyr and oxidation (+15.994915 Da) on Met. A target-decoy database search strategy (Elias and Gygi, 2007) enabled thresholding of the false discovery rate (FDR) for MS/MS spectral assignment at 1%. Correct spectral matches were distinguished from incorrect matches using linear discriminant analysis based on parameters including Xcorr, ΔCn, precursor mass error, peptide length, and charge state (Huttlin et al., 2010). The localizations of individual phosphorylations were assigned using the probability-based AScore algorithm (Beausoleil et al., 2006) and only phosphosites with AScores greater than 13 ($p < 0.05$) were considered in our analysis. Moreover, only phosphopeptides with isolation specificity greater than 0.75 were considered for further analysis. Further filtering of the dataset resulted in a final protein FDR of ~2% and a peptide FDR near 0.15%. TMT labeling was >98% efficient. For TMT reporter ion quantification, a 0.03 Da window centered on the expected mass of each reporter ion was monitored and the intensity of the signal closest to the expected mass was recorded. Reporter ion signals were further adjusted to correct for impurities associated with each TMT label, as described elsewhere (McAlister et al., 2012). Raw TMT reporter ion intensities for individual phosphopeptides were normalized to the summed reporter ion intensity for each TMT label. Adjusted reporter ion intensities were averaged between replicates. Only phosphopeptides for which the summed signal intensity, corrected for noise, among all channels was equal to or greater than 100

were considered. Further, phosphopeptide consideration required signal detection in a least five of six TMT channels for single genotype experiments, and four of six TMT channels for experiments with duplicate samples. Peptides generating detectable TMT reporter ions in only one replicate sample were excluded. A website to query proteins and view identified phosphosites and their levels in kinase-deficient conditions can be found at http://www.flyrnai.org/PhosphoSite.html. Proteomics data have been submitted to the PRIDE Archive repository via ProteomeXchange.

Maternal phenotype derivation

In order to examine maternal phenotypes, 10 maternal-GAL4>UAS-shRNA females, derived from a cross between maternal-GAL4 females and UAS-shRNA bearing males, were crossed to 5 UAS-shRNA males and embryos collected at 27^0C. Hatch rate was calculated based on the ratio of hatched to unhatched embryos, from counting approximately one hundred embryos twenty-four hours after egg deposition. For those genotypes with defective hatching, cuticles were prepared to examine patterning defects using Hoyer's mounting media. Imaging was with a Zeiss Axiophot microscope mounted with a Zeiss AxioCam HRC Camera.

Co-immunoprecipitations

Drosophila cells transfected (Qiagen Effectene Transfection Reagent) with pAHW-Wee together with candidate Wee substrates in pAFW or pAWF were lysed in TNTE lysis buffer (50mM Tris-HCl pH 7.4, 150mM sodium chloride, 1mM EDTA, 0.5% Triton X-100, 1mM sodium fluoride, 1mM β-glycerophosphate, 1mM sodium orthovanadate, 10mM sodium pyrophosphate, 1mM PMSF, EDTA-free Protease Inhibitor Cocktail Tablet (Roche) on ice. Clarified lysates were subjected to immunoprecipitation for 2 hours with anti-FLAG antibody (Sigma F3165) and Protein G Sepharose (GE Healthcare), or HA-agarose (Sigma A2095) for 1 hour at 4^0C. Immunoprecipitates were washed 5x with wash buffer (50mM Tris-HCl pH 7.4, 150mM sodium chloride, 1mM EDTA, 0.1% Triton X-100), boiled in 3x SDS loading buffer, and analyzed by immunoblotting with anti-HA-HRP (Sigma H6533) and anti-FLAG-HRP (Sigma A8592) antibodies. To probe whether Wee expression alters Stwl Tyrosine phosphorylation, clarified lysate were subjected to immunoprecipitation for 2 hours with anti-pTyr antibody (Cell Signaling #9411) and Protein G Sepharose (GE Healthcare) for 1 hour at 4^0C.

Transcript knockdown assessment in cells

Drosophila S2R+ cells were cultured in in Schneider's Medium (Gibco) supplemented with Fetal Bovine Serum (FBS) (final concentration of 10%), Penicillin (50 units/milliliter final concentration), and Streptomycin (50 micrograms/milliliter final concentration). All dsRNA experiments were performed using the bathing method described at www.flyrnai.org. Briefly, S2R+ cells were re-suspended and diluted in serum free medium before seeding with dsRNAs targeting *slik* (DRSC37061) or EGFP. After 30 minutes incubation, complete medium with FBS was added. Cells were harvested following four days of RNAi.

In vitro kinase assay

40 nanograms of recombinant human Wee1 kinase (Invitrogen) was incubated with 100 nanograms of truncated versions of Stwl: amino acids 97-375 (Y305 fragment), amino acids 1-375 (SANT domain + Y305 fragment), amino acids 376-690 (BESS motif), amino acids 690-1037 (Cterm). All Stwl truncations were expressed as N-terminal 6x His fusions in *Escherichia coli* and purified using HisPur Ni-NTA resin. 100 nanograms of recombinant human histone H2B was included as a positive control. Kinase reactions were performed in 20 microliter volumes containing 50 mM Tris-HCl at pH 7.5, 10 mM magnesium chloride, 1 mM dithiothreitol, and 200uM ATP, for 20 minutes at 30°C. Reactions were stopped by addition of 2x sample buffer. Samples were resolved by SDS-PAGE and analyzed by immunoblotting with anti-pTyr (Cell Signaling #9416).

Correlative analysis

Correlative analysis was adapted from (Vinayagam et al., 2013). Briefly, for each phosphosite in a kinase-deficient phosphorylation profile we computed a log2 fold-change value compared to the white shRNA control. The phosphosites with significant increase (≥ 0.58 log2 fold change) or decrease (≤ -0.58 log2 fold change) were distinguished with values +1 and -1 respectively. Phosphosites that did not show significant change ($-0.585 > x < 0.585$) were assigned a value of zero. We constructed a phosphosite matrix by combining multiple kinase-deficient phosphorylation profiles, where the rows correspond to phosphosites and columns correspond to the kinase-deficient datasets. Next, we analyzed all pair-wise combinations of phosphosites to compute the correlation. In a given dataset, if both phosphosites have non-zero values, then the relationship is classified as either positive correlation (both +1 or both -1) or negative correlation (one is +1 and the other is -1). For each pair of phosphosites, we computed the total number of positive and negative correlations. Then we used a simple model to calculate a correlation sign score (CSscore) for each pair of phosphosites as follows:

$$CS_{score} = \frac{P_c - N_c}{T_p} \sqrt{T_p}$$

Pc, Nc corresponds to the number of positive and negative correlations, respectively. Tp is the total number of kinase-deficient phosphorylation profiles where both phosphosites show significant change (Pc + Nc). Note that Tp should be ≥ 2 in order to be considered for correlation analysis. √Tp is the weight factor to assign more confidence for sign correlations predicted based on a larger number of kinase-deficient data. If a score has a positive value (CSscore ≥ 1) then the pair is primarily positive correlated, if the score has negative value (CSscore ≤ -1) then the pair is primarily negatively correlated. The significance of overlap between the correlation network and the reference networks (NetPhorest and Yeast Gold Standard set) was computed using the random overlap (RD), estimated from random correlation networks. To generate a random correlation network the phosphosite matrix was randomized, where the phosphosite signatures are preserved but the phosphosites (IDs) are randomly permuted. Note that we preserved the same number of correlations for kinase phosphosites. Mean and standard deviation of RD is computed from 1,000 simulations of random networks. The p-value is computed by modeling the RD distribution as a Gaussian distribution.

Partial Complementarity Matching of shRNAs

In order to evaluate off-target effects caused by seed-region matches of shRNA reagents, we: 1) extracted the seed sequences of each shRNA reagent, defined as the seven nucleotide sequence between positions 2-8 on anti-sense strand; 2) compared the shRNA seed sequences with the 3UTR or full transcript sequences of genes encoding phosphoproteins downregulated in corresponding shRNA-expressing embryos, considering different levels of confidence; and 3) calculated enrichment P-values based on hyper-geometric distribution. The analysis indicates that the likelihood of phosphoprotein downregulation as a result of transcript degradation due to targeting of the corresponding transcript by the shRNA reagent itself is small is most cases (P-values > 1). Specifically, as the number of downregulated phosphosites for any one protein increases (compare Type 2 and Type 3 phosphoproteins: majority versus all identified phosphosites downregulated respectively), the less likely are off-target effects due to seed-region matches.

Probability of partial complementarity of kinase-targeting shRNAs

	P value (3UTR match)			P value (transcript match)		
downregulated phosphopeps/protein	≥1	≥ 2 Type 2	All Type 3	≥1	≥ 2 Type 2	All Type 3
Atg1 shRNA	0.04126	0.08189	1	0.01875	0.15333	1
Bub1 shRNA	0.30481	1	NA	0.68358	1	NA
cdc2rk shRNA	0.24071	NA	NA	0.21613	NA	NA
Cdk8 shRNA	0.77181	0.48833	1	0.00103	0.00919	0.93122
CG3608 shRNA	0.54999	0.34769	1	0.02582	0.038	1
Cks30A shRNA	0.41284	0.08455	0.75632	0.05222	0.15812	0.76493
Csk shRNA	0.05961	0.62779	0.25645	0.00073	0.09238	0.59762
Eip63E shRNA	0.62702	1	1	0.18518	0.87547	0.5652
gish shRNA	0.10171	1	1	0.00034	0.64949	0.1185
Gprk2 shRNA	2.5E-10	0.00047	1	1	0.91772	1
grp shRNA	0.73225	1	1	0.3602	1	1
Ikb1 shRNA	0.07638	1	1	0.00338	0.19877	1
mei-41 shRNA	0.30451	0.34915	1	0.00405	0.09421	0.93948
mos shRNA	0.01545	0.70575	0.34624	0.00659	0.18434	0.01225
Pak shRNA	0.98115	1	1	0.02103	0.2778	0.43271
slik shRNA	0.10608	1	1	0.00288	0.15739	0.74567
Tao shRNA	0.59414	1	NA	0.00087	0.2447	NA
tefu shRNA	0.51184	0.44943	1	0.12622	0.2193	1
wee shRNA	0.64833	0.87213	1	0.09016	0.28393	0.2984

Germline-specific knockdown of ten candidate off-targets predicted for six kinase-targeting shRNAs

Candidate off-target	Kinase Targeted	Phospho-protein Type	count 7mer trx match	count 7mer 3UTR match	Bloomington shRNA stock #	candidate off-target phenotype?	Match kinase phenotype?
Rfabg	Atg1	Type 3	3	2	28946	F1 lethal	
Ptr	Pak	Type 3	3		no line exists		
Smg5	gish	Type 3	6		no line exists		
Smg5	mos	Type 3	3		no line exists		
Etl1	mos	Type 3	1	1	33891	No	No
Bx42	slik	Type 3	1		34777	no eggs	No
GAPcenA	wee	Type 3	2		34976	No	No
garz	mos	Type 3	2		34987	no eggs	No
jumu	Cks30A	Type 3	1		no line exists		
retn	gish	Type 3	1		35688	No	No
Mlc2	Csk	Type 3	1	1	36694	F1 lethal	
MRP	Cks30A	Type 3	3		38316	No	No
slpr	Cdk8	Type 3	3		41605	dorsal closure defects	No
CycB3	Eip63E	Type 3	1		no line exists		
Dab	gish	Type 3	2		42646	No	No
CG4004	Cks30A	Type 3	1	1	no line exists		
CG5728	wee	Type 3	1	1	36592	No	No
poe	wee	Type 3	1		32945	no eggs	No

References

Amoutzias, G.D., He, Y., Lilley, K.S., Van de Peer, Y., and Oliver, S.G. (2012). Evaluation and properties of the budding yeast phosphoproteome. Mol Cell Proteomics *11*, M111 009555.

Beausoleil, S.A., Villen, J., Gerber, S.A., Rush, J., and Gygi, S.P. (2006). A probability-based approach for high-throughput protein phosphorylation analysis and site localization. Nat Biotechnol *24*, 1285-1292.

Brunner, E., Ahrens, C.H., Mohanty, S., Baetschmann, H., Loevenich, S., Potthast, F., Deutsch, E.W., Panse, C., de Lichtenberg, U., Rinner, O*., et al.* (2007). A high-quality catalog of the Drosophila melanogaster proteome. Nat Biotechnol *25*, 576-583.

Chou, M.F., and Schwartz, D. (2011). Biological sequence motif discovery using motif-x. Current protocols in bioinformatics / editoral board, Andreas D Baxevanis [et al] *Chapter 13*, Unit 13 15-24.

Dephoure, N., Zhou, C., Villen, J., Beausoleil, S.A., Bakalarski, C.E., Elledge, S.J., and Gygi, S.P. (2008). A quantitative atlas of mitotic phosphorylation. Proc Natl Acad Sci U S A *105*, 10762-10767.

Elias, J.E., and Gygi, S.P. (2007). Target-decoy search strategy for increased confidence in large-scale protein identifications by mass spectrometry. Nat Methods *4*, 207-214.

Eng, J.K.M., A.L., Yates, J.R., 3rd (1994). An Approach to Correlate Tandem Mass Spectral Data of Peptides with Amino Acid Sequences in a Protein Database. J Am Soc Mass Spectrom *5*, 976-989.

Groth, A.C., Fish, M., Nusse, R., and Calos, M.P. (2004). Construction of transgenic Drosophila by using the site-specific integrase from phage phiC31. Genetics *166*, 1775-1782.

Huttlin, E.L., Jedrychowski, M.P., Elias, J.E., Goswami, T., Rad, R., Beausoleil, S.A., Villen, J., Haas, W., Sowa, M.E., and Gygi, S.P. (2010). A tissue-specific atlas of mouse protein phosphorylation and expression. Cell *143*, 1174-1189.

Kettenbach, A.N., and Gerber, S.A. (2011). Rapid and reproducible single-stage phosphopeptide enrichment of complex peptide mixtures: application to general and phosphotyrosine-specific phosphoproteomics experiments. Anal Chem *83*, 7635-7644.

McAlister, G.C., Huttlin, E.L., Haas, W., Ting, L., Jedrychowski, M.P., Rogers, J.C., Kuhn, K., Pike, I., Grothe, R.A., Blethrow, J.D*., et al.* (2012). Increasing the multiplexing capacity of TMTs using reporter ion isotopologues with isobaric masses. Anal Chem *84*, 7469-7478.

Olsen, J.V., Macek, B., Lange, O., Makarov, A., Horning, S., and Mann, M. (2007). Higher-energy C-trap dissociation for peptide modification analysis. Nat Methods *4*, 709-712.

Petrella, L.N., Smith-Leiker, T., and Cooley, L. (2007). The Ovhts polyprotein is cleaved to produce fusome and ring canal proteins required for Drosophila oogenesis. Development *134*, 703-712.

Rajan, A., and Perrimon, N. (2013). Of flies and men: insights on organismal metabolism from fruit flies. BMC Biol *11*, 38.

Rappsilber, J., Ishihama, Y., and Mann, M. (2003). Stop and go extraction tips for matrix-assisted laser desorption/ionization, nanoelectrospray, and LC/MS sample pretreatment in proteomics. Anal Chem *75*, 663-670.

Thomason, L.C., Calendar, R., and Ow, D.W. (2001). Gene insertion and replacement in Schizosaccharomyces pombe mediated by the Streptomyces bacteriophage phiC31 site-specific recombination system. Mol Genet Genomics *265*, 1031-1038.

Ting, L., Rad, R., Gygi, S.P., and Haas, W. (2011). MS3 eliminates ratio distortion in isobaric multiplexed quantitative proteomics. Nat Methods *8*, 937-940.

Villen, J., and Gygi, S.P. (2008). The SCX/IMAC enrichment approach for global phosphorylation analysis by mass spectrometry. Nat Protoc *3*, 1630-1638.

Vinayagam, A., Zirin, J., Roesel, C., Hu, Y., Yilmazel, B., Samsonova, A.A., Neumuller, R.A., Mohr, S.E., and Perrimon, N. (2013). Integrating protein-protein interaction networks with phenotypes reveals signs of interactions. Nat Methods.